Testing the Simple Biosphere Model (SiB) Using Point Micrometeorological and Biophysical Data

P. J. SELLERS AND J. L. DORMAN

Center for Ocean–Land–Atmosphere Interactions, Department of Meteorology, University of Maryland, College Park, MD 20742

(Manuscript received 10 January 1986, in final form 20 November 1986)

ABSTRACT

The Simple Biosphere model (SiB) of Sellers et al. (1986) was designed for use within General Circulation Models (GCMs) of the earth's atmosphere. The main objective of SiB is to provide a biophysically realistic description of those processes which control the transfer of radiation, sensible heat, latent heat and momentum between the terrestrial surface and the atmosphere. As a result, SiB is more complex and has a larger input parameter set than most equivalent formulations used in GCMs. Prior to implementing SiB in a GCM, it is essential that its components and its functioning as a whole be thoroughly tested. Additionally, it is highly desirable that the model's response to errors or uncertainties in the input parameter set be explored. This paper discusses investigations that were directed at addressing these two issues.

Micrometeorological and biophysical measurements from surface experiments conducted over arable crops in West Germany and the United States and a forested site in the United Kingdom were used to test the operation of SiB. Observed values of the downward radiative fluxes, wind speed, air temperature and water vapor pressure recorded above the surface were used as the boundary forcing for the SiB model. The predicted partitioning of the absorbed radiation into the sensible and latent heat fluxes compares well with observations and the various subcomponents of the model appear to operate realistically. The sensitivity of the model's energy balance calculations to changes in the various model parameters and the soil moisture initialization is examined. It is estimated that the model will generate uncertainties of the order of ±7% in the calculated net radiation, and up to ± 25% in the calculated evapotranspiration rate, with typical values of ±15%.

1. Introduction

The Simple Biosphere model (SiB) was designed for use within General Circulation Models (GCMs) of the earth's atmosphere. A full description of the philosophy, design and requirements of the model may be found in Sellers et al. (1986) so only a brief review will be presented here.

Until the work of Dickinson (1984), land surface parameterizations in GCMs took little or no account of biophysical processes: albedo, surface roughness and energy partition properties were specified independently for each terrestrial grid area and simple empirical functions were used to regulate the depletion of the soil moisture store by evapotranspiration (see Sellers, 1987). The work of Dickinson (1984) and Sellers et al. (1986) has been directed at constructing biophysically realistic models which aim to model the vegetation itself and thereby calculate consistent reflectance, drag and energy partition characteristics for a given vegetated surface. Besides working towards the goal of improved realism, it is hoped that this biophysical modeling approach will also result in more accurate predictions of the various surface fluxes.

Biophysical models are, by necessity, more complicated than their mainly empirical predecessors. As a result, these models have a much larger number of parameters to define the characteristics of a given grid area: for example, a vegetation–soil complex in SiB is characterized by around 50 parameters as compared with the three to five parameters used in earlier models. This larger parameter set consists of physically measurable quantities, some of which may be obtained via remote sensing, rather than loosely defined conceptual parameters which are somewhat divorced from biophysical reality. Clearly the compilation of such a large parameter set presents us with a significant practical problem, particularly if no priorities or accuracy requirements can be attached to any of the component parameters. It is highly desirable that in addition to evaluating the model's performance prior to its installation in a GCM, some sensitivity study be executed so that the relative importance of the constituent parameters can be assessed. The work presented in this paper therefore has two aims: first, a test of the model's operation and, second, a sensitivity study to assess the accuracy requirements for the parameter set. The methods used to pursue these aims are discussed in sections 3 and 4, respectively.

A thorough evaluation of the performance of the various subcomponents of the model and their functioning as a complete ensemble is essential prior to implementing SiB in a GCM where unanticipated feedbacks between the boundary layer and surface

models might obscure serious errors in the formulation. This paper discusses some results of testing the performance of SiB in isolation from a GCM. In these tests, the upper boundary conditions, which are normally taken as the meteorological and radiation conditions in the lowest layer of the GCM, were provided by micrometeorological measurements recorded a few meters above the surface.

Few experimental studies have been conducted in vegetated sites where all of the variables necessary to force and validate the SiB model were measured. To date, we have managed to obtain the requisite data only for some agricultural sites in West Germany and the United States and for a forested site in Central Wales, United Kingdom. Accordingly, the model parameters were fixed to represent barley, wheat and maize crops, and a coniferous forest cover for which the necessary data sets were available (Tables 1 and 2). The morphological and physiological properties of the vegetation and the physical properties of the vegetation and soil (see Table 1 in Sellers et al., 1986) were measured or estimated for the experimental sites and were used to derive the model's surface parameters. Soil moisture contents were initialized from observations and adjusted prognostically thereafter. The micrometeorological measurements were applied as the boundary forcing to the model and time series of the radiation exchanges, heat fluxes and surface temperatures generated.

The first part of this paper presents the results of these simulations. In general, the predicted values of the sensible and latent heat fluxes, surface temperatures and other biophysical variables concur with observations.

In the second part of the paper, the sensitivity of the model energy balance calculations to changes in the values of the surface parameters is discussed in some detail. It can be assumed that the large-scale parameter sets currently being assembled for the implementation of SiB into a GCM will be subject to large uncertainties in some of their constituent values. The consequences of including errors of different types in such a model may be explored by such sensitivity analyses. Additionally, the data research effort may be concentrated on providing accurate estimates of those parameters to which the model is particularly sensitive. The sensitivity studies should also allow us to assess the influence of subgrid-scale variability on the values of the calculated fluxes returned to the model atmosphere.

Before moving on to a discussion of the results of these studies, we present a brief description of the structure and operation of SiB.

2. The Simple Biosphere model (SiB)

The structure of the model is shown schematically in Fig. 1. Essentially, the upper-story canopy and ground surface are considered to interact with conditions in the canopy air space via two aerodynamic resistances: the bulk boundary layer resistance, $\overline{r_b}$, and the ground-to-canopy air space resistance, r_d; and three surface resistances: $\overline{r_c}$, r_g and r_{surf} which relate to the upper-story canopy, ground cover and soil, respectively. (The overbars in $\overline{r_c}$ and $\overline{r_b}$ mean that these terms are area-averages.) When the foliage is dry, the canopy resistances $\overline{r_c}$ and $\overline{r_b}$ are calculated by assuming that all the individual stomatal and boundary layer leaf resistances act in parallel. A modified two-stream radiative transfer approximation, as described in Dickinson (1983) and Sellers (1985), is used to calculate the amount of downward radiation absorbed by the canopy and ground over the visible, or photosynthetically active, (0.4–0.7 μm) and near-infrared (>0.7 μm) solar wavelength intervals. Longwave radiation losses are calculated and subtracted from the total absorbed radiation to yield estimates of the net radiation for the canopy and ground. It is necessary to have discrete estimates of the downward visible (direct and diffuse),

TABLE 1. Properties of the crops and soil at the test sites. All values were obtained from van der Ploeg et al. (1980) for wheat and barley, Choudhury (1983) for maize, and Calder and Harding (personal communication) and Jarvis (1976) for spruce except for some of the following: z_1, z_s and V_c were estimated; values of χ_L from Ross (1975); C_d and C_s from Goudriaan (1977) and Wilson et al. (1982); p_s from Thom (1972) and Wilson et al. (1982); r_{plant} estimated from data of Denmead (1976) and ranges from 2.2E8 to 4.0E8 s; R_r from Denmead (1976), Newman (1969) and Newman (1973); leaf optical properties from Goudriaan (1977) and Dickinson (1983); a, b and c from fitting to data of Monteith et al. (1965), Denmead (1976), Turner (1974), Korner et al. (1979) and Jarvis (1976); ψ_{c_1} and ψ_{c_2} from data of Frank et al. (1973), Millar et al. (1970), Reicosky and Lambert (1978) and Jarvis (1976); soil physical properties from Clapp and Hornberger (1978). N.B. Jarvis (1976) data applies to Sitka spruce, not Norway spruce.

		Soil			
Soil moisture potential at saturation	ψ_s (m)	−1.60	−1.60	−0.48	−0.48
Soil moisture potential parameter	B	2.80	2.80	5.39	5.39
Soil saturation cond.	K_s (m s^{-1})	2.89E-5	2.89E-5	6.95E-6	6.95E-6
Porosity	θ_s	0.43	0.43	0.45	0.45
Soil moisture store depths	D_1, D_2, D_3 (m)	0.02, 0.58, 0.60	0.02, 0.58, 0.60	0.02, 0.98, 1.0	0.02, 0.18, 0.40
Soil reflectance (VIS, NIR)	α_s	0.08, 0.18	0.08, 0.18	0.10, 0.20	0.10, 0.20

TABLE 2. Micrometeorological and other time series data used to force the SiB model for (A) wheat and barley crops (Gurney and Camillo, 1984; van der Ploeg et al., 1980), (B) maize crop (Choudhury, 1983), and (C) Norway spruce (Calder and Harding, personal communication). All micrometeorological data were recorded hourly or more frequently; T_r, T_w and u are air temperature, wet bulb temperature and wind speed recorded 2 m above surface; $S\downarrow$, $LW\downarrow$ and R_n are downward solar, longwave and net radiation, respectively; λE and H are the latent and sensible heat fluxes (estimated via the Bowen ratio), G is the ground heat flux, T_s is the surface radiometric temperature, T_1 is the soil temperature at 1 cm depth, P_0 and P_L are the rainfall rates above and below the canopy, W is the soil moisture, r_s is leaf stomatal resistance and ψ_l is the leaf water potential.

Parameter	Units	Barley	Wheat	Maize	Spruce
		Vegetation			
Height of canopy top	z_2 (m)	1.02	0.80	1.20	10.0
Height of canopy base	z_1 (m)	0.05	0.05	0.10	4.0
Ground roughness length	z_s (m)	0.005	0.005	0.005	0.005
Leaf area index	$\bar{L_l}$	3.72	6.2	3.5–4.2	8.4
Leaf angle distribution factor	χ_L	0.09	−0.02	0.01	0.01
Leaf drag coefficient	C_D	0.098	0.11	0.10	0.13
Leaf shelter factor	p_s	2.9	5.1	2.6–2.9	1.7
Upper story cover fraction	V_c	1.0	1.0	1.0	1.0
Root density	D_d (mm^{-3})	3600	2910	5000	3600
Root depth	z_d (m)	1.15	0.95	1.0	0.58
Root cross section	(m^2)	3.84E-7	3.84E-7	1.5E-5	3.84E-7
Root resistance	R (s ms^{-1})	4.0E12	4.0E12	4.0E12	4.0E12
Stem resistance	$\overline{r_{\text{plant}}}$ (s)	2.5E8	2.5E8	2.5E8	2.5E8
Leaf reflectance (VIS, NIR)	α	0.105, 0.578	0.105, 0.578	0.105, 0.578	0.07, 0.5
Leaf transmission (VIS, NIR)	δ	0.070, 0.248	0.070, 0.248	0.070, 0.248	0.07, 0.248
		Stomatal Resistance			
Light parameters	a, b, c	2333, 20.9, 55.	7450., 5.7, 25.2	17500., 6.0, 110.	2869, 3.6, 232.5
Leaf water potential parameters	ψ_{c_1}, ψ_{c_2} (m)	−70., −140.	−100., −200.	−100., −220.	
Temperature parameters	T_1, T_h, T_0 (K)	....	268, 300, 315	....	268, 283, 316

	T_r	T_w	u	$S\downarrow$	$LW\downarrow$	R_n	G	λE	H	T_s	T_1	P_0	P_L	W	r_s	ψ_l
(A) Bare soil (Near Site I)	✓	✓	✓	✓	✓	✓	✓				✓					
Barley I	✓	✓				✓	✓	✓	✓					✓	✓	
Barley II	✓	✓	✓	✓		✓	✓			✓						
Wheat III	✓	✓	✓	✓		✓	✓									
(B) Maize	✓	✓	✓	✓										✓		✓
(C) Norway spruce	✓	✓	✓	✓		✓						✓	✓	✓		

near-infrared (direct and diffuse) and thermal infrared (assumed to be all diffuse) radiation. The soil heat flux is modeled simply by using a slab model; that is, the ground is taken to be *thermally* equivalent to a layer of water of uniform temperature with the depth of the layer varying from 25 to 40 mm depending on soil wetness—this is in accordance with the practice used in early versions of the Goddard Laboratory of Atmospheric Sciences GCM (see Arakawa, 1972).

The net radiation absorbed by the canopy and soil is assumed to be partitioned into sensible heat, latent heat and storage terms as

$$Rn_c = \lambda E_c + H_c + C_c \frac{\partial T_c}{\partial t} \tag{1}$$

$$Rn_{gs} = \lambda E_{gs} + H_{gs} + C_{gs} \frac{\partial T_{gs}}{\partial t} \tag{2}$$

where

T_c, T_{gs} surface temperature, K
C_c, C_{gs} heat capacity, J K^{-1} m^{-2}
Rn_c, Rn_{gs} net radiation, W m^{-2}
λE_c, λE_{gs} evapotranspiration flux, W m^{-2}
H_c, H_{gs} sensible heat flux, W m^{-2}.

The subscripts c, g and s refer to the upper-story canopy, ground vegetation and soil, respectively. The combined subscript gs refers to both ground cover and soil.

The fluxes of sensible and latent heat from the canopy and ground are represented by electrical analogue

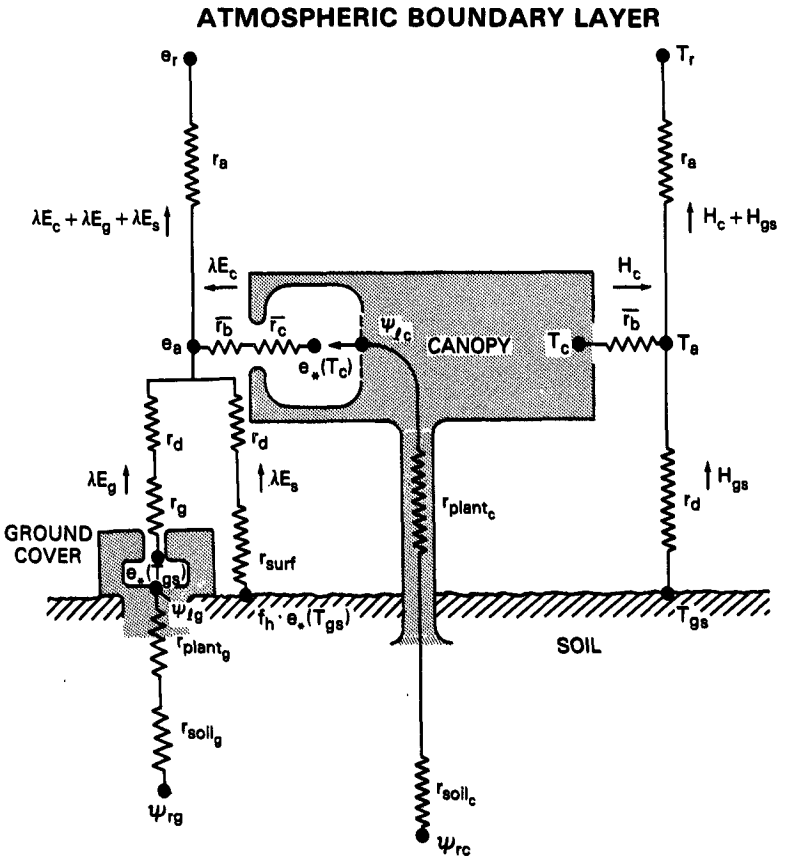

FIG. 1. Schematic diagram of the Simple Biosphere model (SiB). The transfer pathways for latent and sensible heat are shown on the left- and right-hand sides of the diagram, respectively.

models in which the fluxes are proportional to potential differences (in temperature or vapor pressure) and inversely proportional to resistances, which are equivalent to the inverse integrals of conductances over a specified length scale. For example, an aerodynamic resistance is calculated by integrating the inverse of a turbulent diffusion coefficient between two reference points. Reference to Fig. 1 and Sellers et al. (1986) will show that these heat fluxes may be written as follows:

$$\lambda E_c = [e*(T_c) - e_a]\frac{\rho c_p}{\gamma}\left(\frac{W_c}{\bar{r}_b} + \frac{1 - W_c}{\bar{r}_c + \bar{r}_b}\right) \quad (3)$$

where

$e*(T_c)$ saturated vapor pressure at temperature T_c, mb
e_a canopy air space vapor pressure, mb
ρ, c_p density and specific heat of air, kg m^{-3}, J kg^{-1} K^{-1}
W_c canopy wetness fraction
$\bar{r}_c$ bulk canopy stomatal resistance, s m^{-1}
$\bar{r}_b$ bulk canopy boundary layer resistance, s m^{-1}
γ psychrometric constant, mb K^{-1}.

$$\lambda E_{gs} = [e*(T_{gs}) - e_a] \times \frac{\rho c_p}{\gamma}\left[V_g\left(\frac{W_g}{r_d} + \frac{1 - W_g}{r_d + r_g}\right) + \frac{(1 - V_g)}{r_{surf} + r_d}h_s\right] \quad (4)$$

where

$e*(T_{gs})$ saturated vapor pressure at temperature, T_{gs}, mb
r_g bulk ground vegetation stomatal resistance, s m^{-1}
r_{surf} soil surface resistance, s m^{-1}
r_d aerodynamic resistance between soil surface and canopy air space, s m^{-1}
V_g ground vegetation cover fraction
W_g ground vegetation wetness fraction
h_s factor to correct for soil dryness.

$$H_c = \frac{2(T_c - T_a)}{\bar{r}_b}\rho c_p \quad (5)$$

$$H_{gs} = \frac{(T_{gs} - T_a)}{r_d}\rho c_p \quad (6)$$

where

T_a canopy air space temperature, K.

The latent and sensible heat fluxes from the soil and canopy combine to give the total surface fluxes, which are transferred from the canopy air space to the reference height, z_r, and are given by

$$\lambda E_c + \lambda E_{gs} = \frac{(e_a - e_r)}{r_a} \frac{\rho c_p}{\gamma} \tag{7}$$

$$H_c + H_{gs} = \frac{(T_a - T_r)}{r_a} \rho c_p \tag{8}$$

where

e_r vapor pressure at reference height, mb
T_r air temperature at reference height, K
r_a aerodynamic resistance, s m^{-1}.

Substituting (3) to (8) into (1) and (2) yields two differential equations in T_c and T_{gs}. These are solved simultaneously using a backwards implicit method.

Most of the calculations carried out in SiB originate from three submodels. First, the radiative transfer submodel calculates the net radiation terms, Rn_c and Rn_{gs}, that make up the right-hand sides of (1) and (2). The aerodynamic resistance submodel calculates the values of $\overline{r_b}$, r_d and r_a which are used in (3) to (8) to govern the transport of heat and water vapor through the air. The surface resistance submodel calculates the values of $\overline{r_c}$, r_g and r_{surf}, which are used in (3) to (8) to control the passage of water from within the plant leaves or the top soil layer to the exterior air.

In order for the model to simulate surface processes well, each of its three subcomponents, namely radiative transfer, aerodynamic resistances (turbulent transfer) and surface resistances (biophysical control of evapotranspiration) must be demonstrably realistic and accurate. In sections 3–5 we describe the experimental sites, the derivation of the model parameters and the performance of the various submodels.

3. Evaluation of model performance

In this section, we evaluate the SiB model's performance in terms of its ability to realistically and accurately simulate biophysical processes over a number of test sites for which data were available for validation. First, we describe the experimental sites and the types of data that were available for each one. Second, we briefly review the structure and performance of each of the three submodels that go to make up SiB. Third, we describe the results of simulation runs conducted for each of the test sites and compare them with observations.

a. The test sites

Data from two agricultural sites and one forested site were available for the evaluation of SiB.

- *Site A:* Ruthe, Federal Republic of Germany, 19–21 June 1979

A full description of the site and observing systems used in the Joint Measuring Campaign of 1979 at Ruthe, Federal Republic of Germany, can be found in Gurney and Camillo (1984) and van der Ploeg et al. (1980). A number of institutions cooperated to measure micrometeorological, biophysical, pedological and radiative variables in an agricultural area 15 km south of Hannover. The data used for this simulation study were recorded over wheat, barley and bare soil plots and are listed in Table 1. Data were recorded over two barley fields, here referred to as Plots I and II, one wheat field, Plot III, adjacent to barley Plot II and a bare soil plot.

- *Site B:* South Carolina, United States

A field of maize was studied throughout a growing season (see Reicosky et al., 1975; Reicosky and Lambert, 1978). The data for two selected days were used subsequently by Choudhury (1983) to test a soil–plant–atmosphere model with particular emphasis on the relationships between leaf water potential and evapotranspiration rate. The same data (see Table 1) were used to test the leaf water potential component of SiB.

- *Site C:* Central Wales, United Kingdom

A forested catchment near Plynlimon, Central Wales has been the subject of some intensive study by researchers operating from the Institute of Hydrology (IH), United Kingdom. Calder (1976), (1977) and (1978) and Calder and Newson (1979) have described the design of the IH natural lysimeter, where the water balance of a small forested area was monitored over a period of nearly 2 yr. The technique involved isolating a stand of 27 mature Norway spruce trees from lateral water exchange by grouting an encircling wall of steel sheets into the effectively waterproof layer of clay underlying the site. Measurements of rainfall above and below the canopy and of the changes in soil moisture in the isolated soil block allowed the researchers to calculate interception loss, soil evaporation and canopy transpiration rates. Hourly micrometeorological measurements (air temperature and humidity, wind speed, net radiation, global incoming radiation) were recorded in a clearing a short distance away from the site and the values adjusted to synthesize an equivalent data set above the canopy.

Since both agricultural sites (sites A and B) were involved with studies of processes associated with uniform, monoculture vegetation, it was not possible to perform a test of SiB in its full form as specified in Sellers et al. (1986), that is, with an upper-story canopy and underlying ground vegetation. In both cases, we have "promoted" the crop canopy to the status of upper-story vegetation and have taken the ground surface as bare so that $V_g = 0$.

b. Submodel performance

1) RADIATIVE TRANSFER SUBMODEL

A two-stream approximation model of radiative transfer is used with the scattering parameters specified as in Dickinson (1983),

$$-\bar{\mu}\frac{dI\uparrow}{dL}+[1-(1-\beta)\omega]I\uparrow-\omega\beta I\downarrow=\omega\bar{\mu}K\beta_0 e^{-KL} \quad (9)$$

$$\bar{\mu}\frac{dI\downarrow}{dL}+[1-(1-\beta)\omega]I\downarrow-\omega\beta I\uparrow=\omega\bar{\mu}K(1-\beta_0)e^{-KL} \quad (10)$$

where

$I\uparrow, I\downarrow$	upward and downward diffuse radiative fluxes, normalized by the incident solar fluxes
K	optical depth of the direct beam per unit leaf area $[=G(\mu)/\mu]$
$G(\mu)$	Projected area of leaf elements in direction μ
$\mu = \text{Cos}\theta$	Cosine of angle of incident beam
$\bar{\mu}$	average inverse diffuse optical depth per unit leaf area $[=\int_0^1 [\mu'/G(\mu')]d\mu']$
μ'	direction of scattered flux
ω	scattering coefficient
L	cumulative leaf area index.

β and β_0 are the upscatter parameters for the diffuse and incident beams respectively. A number of simplifications are made in SiB in order to obtain the parameters $\bar{\mu}$, β and β_0 for canopies of differing leaf angle distributions (see Sellers et al., 1986; Dickinson, 1983; Sellers, 1985).

The albedo and transmittance of the canopy may be obtained by solving (9) and (10) with suitable boundary conditions. For example, if all of the incoming radiation is direct, then the boundary conditions are

$$\left.\begin{aligned} I\downarrow &= 0 \quad \text{at} \quad L=0 \\ I\uparrow &= \rho_s(I\downarrow + e^{-KL_t}) \quad \text{at} \quad L=L_t \end{aligned}\right\} \quad (11)$$

where

L_t	local leaf area index
ρ_s	soil reflectance.

The bulk radiative properties of the canopy are then given by the solutions to the following equations:

$$\left.\begin{aligned} &\text{Canopy reflectance} = I\uparrow \quad \text{at} \quad L=0 \\ &\text{Canopy transmittance} = I\downarrow + e^{-KL_t} \quad \text{at} \quad L=L_t \end{aligned}\right\} \quad (12)$$

Appropriate boundary conditions and dropping the direct-beam terms on the right-hand sides of (9) and (10) allow us to calculate the partition of incident diffuse fluxes into absorbed, transmitted and reflected components.

Canopy albedo was not measured at any of the experimental sites but observations of total downward and reflected shortwave radiation were made at Volkenrude, some 50 km distant from the Ruthe, West Germany field site, contemporaneously with the field experiments. Figure 2 shows the measured albedo above a winter wheat crop during 20–21 June and the simulated total albedo for the wheat III plot for 20 June. The simulated albedo was calculated by summing the reflected visible and near-infrared radiation fluxes (diffuse and direct) and dividing by the total incoming shortwave flux. The proportions of the various spectral and angular fractions of shortwave income were estimated from the scheme of Goudriaan (1977; Fig. 1, p. 11). It is clear that the model can reproduce both the diurnal variation and the magnitude of the canopy albedo with some realism.

The performance of the radiation submodel in predicting the transmittance of a vegetation canopy was evaluated using another data set; see Sellers (1985).

Further tests have been carried out with the radiation submodel (Sellers, 1985), including some comparisons of the submodel's performance against the output gen-

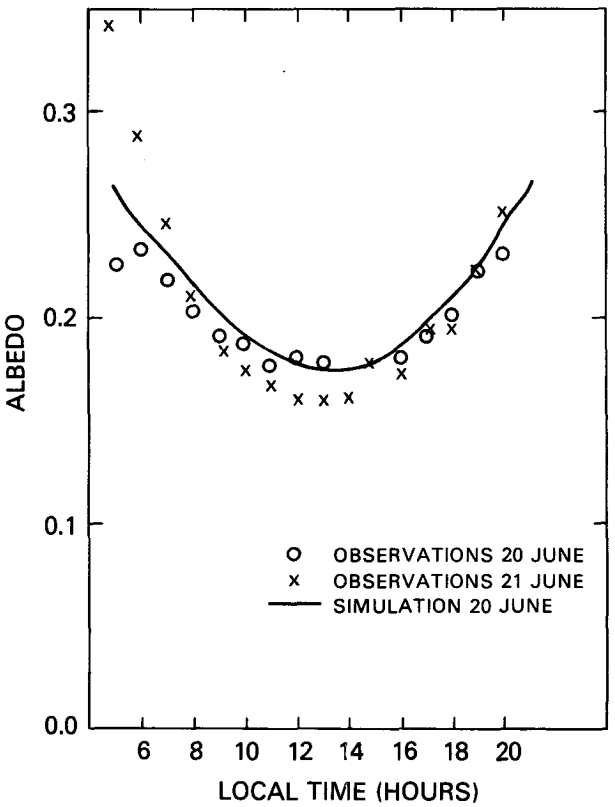

FIG. 2. Measured and simulated albedo values for shortwave radiation above a wheat crop. The observed points were calculated from observations of incoming and outgoing shortwave radiation taken at Volkenrude, W. Germany, 20–21 June 1979. The simulation for the wheat crop at Ruthe (50 km away) for 20 June is also shown.

erated by a numerical ray-tracing model (Kimes et al., 1987). In all cases, the model seems to reproduce the trends exhibited by observations (i.e., the variation of reflectances and/or transmittances with solar angle, leaf orientation, etc.) and does not diverge greatly from equivalent results produced by the more exact numerical models.

2) Aerodynamic resistances submodel

The details of the simple diffusion model used to describe the transport of mass, heat and momentum in SiB are given in Sellers et al. (1986). Briefly, the model links the transfer conditions above the canopy (described by the log-linear profile) to a gradient diffusion model, where K_m, the local momentum transfer coefficient, is assumed to be proportional to the local wind speed. A correction is made to the profile of K_m within the transition layer above the canopy, where observations (see Garratt, 1978) have shown it to be 1.5 to 2 times as great as an estimate obtained from extrapolating the log-linear profile.

Appendix A of Sellers et al. (1986) sets out the details of the solution procedure leading to the estimation of the surface roughness length, z_0, and zero plane displacement height, d. Implicit in this process is the calculation of wind and momentum transfer coefficient profiles which may be integrated to provide estimates of the aerodynamic resistance, r_a, acting between the canopy source height, h_a, ($\sim z_0 + d$) and reference height, z_r; the bulk boundary layer resistance, $\overline{r_b}$, which governs the fluxes of heat and moisture between the bulk upper-story canopy and the surrounding air space; and the ground aerodynamic resistance, r_d, which controls the fluxes of heat and moisture from the soil surface and ground cover to the canopy air space (see Fig. 1).

The solution of the turbulent transfer equation set requires the specification of the following parameters: height of the canopy top, z_2; height of canopy base, z_1; leaf area density, L_d; leaf drag coefficient, C_d; shelter factor, p_s; and the roughness length of the ground, z_{gs}.

It is assumed that the turbulent transfer coefficient for momentum is related to the local wind speed within the canopy by the following simple expression:

$$K_m = \sigma u \tag{13}$$

where

K_m momentum transfer coefficient, $m^2\ s^{-1}$
σ constant, m
u local wind speed, $m\ s^{-1}$.

The value of σ is obtained for a given site by the iterative solution of the equations in Sellers et al. (1986), appendix A, using the specified set of input parameters. The resulting value of σ and the derived variables, z_0 and d, have to satisfy the conditions of continuity of shear stress and wind speed profiles above, within and below the canopy.

The bulk boundary layer resistance to heat and water vapor transfer, $\overline{r_b}$, is then calculated by

$$\frac{1}{\overline{r_b}} = \int_{z_1}^{z_2} \frac{\overline{L_d} u^{1/2}}{p_s C_s}\, dz \tag{14}$$

where

$\overline{L_d}$ area-averaged upper-story canopy leaf area density, $m^2\ m^{-3}$
z_1, z_2 height of canopy base, top respectively, m
p_s canopy shelter factor
C_s leaf transfer coefficient for heat and vapor, $(m\ s^{-1})^{-1/2}$

or, more simply, by

$$\overline{r_b} = \frac{C_1}{\sqrt{u_2}} \tag{15}$$

where

C_1 constant determined from terms on right-hand side of (14), $(m\ s^{-1})^{-1/2}$
u_2 wind speed at canopy top; z_2, $m\ s^{-1}$.

A simple modification for the effects of free convection, based on a consideration of the Nusselt number for leaves (see Monteith, 1973) is combined with (15); see Sellers et al. (1986), appendix A.

Next, the resistance acting between the soil surface and the canopy source height, r_d, is calculated by integrating the inverse of a turbulent transfer coefficient between the ground and the canopy source height, h_a.

$$r_d = \int_{z_{gs}}^{z_1} \frac{1}{K_s}\, dz + \int_{z_1}^{h_a} \frac{1}{K_s}\, dz$$

$$= \frac{1}{u_{(z_1)}} \left[\frac{\ln(z_1/z_{gs})}{k} \right]^2 + \int_{z_1}^{h_a} \frac{1}{\sigma u}\, dz \tag{16}$$

where

k von Karman's constant, 0.41
z_{gs} effective roughness length of the soil surface, m
h_a canopy source height, m
K_s turbulent heat and vapor transfer coefficient, $m^2\ s^{-1}$.

(The canopy source height, h_a, is taken to be the center of aerodynamic drag in the canopy. It was found that estimates of r_a and r_d are fairly insensitive to the exact location of h_a.) Note that K_s is assumed to be equal to K_m in any air volume where turbulent transfer is the dominant transport process, i.e., everywhere except in the leaf laminar boundary layer.

Integration and collection of terms in (16) yields

$$r_d = \frac{C_2}{u_2} \tag{17}$$

where

C_2 constant determined from integration of (16).

This expression for r_d is modified to account for the

effects of free convection under the canopy; see Sellers et al. (1986).

The aerodynamic resistance, r_a, is imposed on the transfer of heat and moisture between h_a and the reference height, z_r. When linking SiB to a GCM, it is preferable to use a modification of the Deardorff (1972) parameterization. However, since the micrometerological data used as the upper boundary conditions in these tests were collected a short distance above the crop (presumably within the constant stress layer) we may use a modified version of the Paulson (1970) parameterization for the description of transfer processes above the canopy.

Firstly, the height of the transition layer, z_m, above the crop is taken to be equivalent to twice the mean obstacle height, $(z_2 - d)$. To take account of the augmentation of the heat transfer coefficient, K_s, within the transition layer, we specify a constant, G_2, which represents the ratio between the actual aerodynamic resistance above the canopy and that value which would be obtained by simply extrapolating the log-linear profile down from z_m to z_2. Thus,

$$\int_{z_2}^{z_m} \frac{1}{K_s} dz = G_2 \int_{z_2}^{z_m} \frac{1}{K_s^*} dz \tag{18}$$

where

K_s "actual" value of K_s, $m^2\ s^{-1}$.
K_s^* value of K_s obtained from log-linear profile, $m^2\ s^{-1}$.

G_2 is estimated to be about 0.5 from observations (see Garratt, 1978 and Raupach and Thom, 1981). We may write the aerodynamic resistance between h_a and z_r as

$$r_a = \int_{h_a}^{z_2} \frac{1}{K_s} dz + \frac{G_2}{ku_*}\left[\log\left(\frac{z_m - d}{z_2 - d}\right) - \psi_{2_{z_2}}{}^{z_m}\right] + \frac{1}{ku_*}\left[\log\left(\frac{z_r - d}{z_m - d}\right) - \psi_{2_{z_m}}{}^{z_r}\right] \tag{19}$$

where

u_* friction velocity, $m\ s^{-1}$
$\psi_{2_{z_b}}^{z_a}$ Paulson (1970) correction coefficient for vapor transfer evaluated between heights z_a and z_b
z_r reference height, m
z_m height of transition layer, m.

The value of the first term on the right in (19), the resistance acting between h_a and z_2, is obtained in a similar manner as r_d. The friction velocity, u_*, is calculated iteratively using modifications of the Paulson (1970) descriptions of the wind profile.

Figure 3 shows the profiles of shear stress and wind speed as observed by Wilson et al. (1982) and as calculated by SiB for a maize crop. Wilson et al. (1982) also made observations of crop height (2.3 m) and leaf area index (2.9) and provided an estimate of the effective leaf drag coefficient (0.17). We have used these data to solve the momentum balance equations described above and in Sellers et al. (1986) and to derive

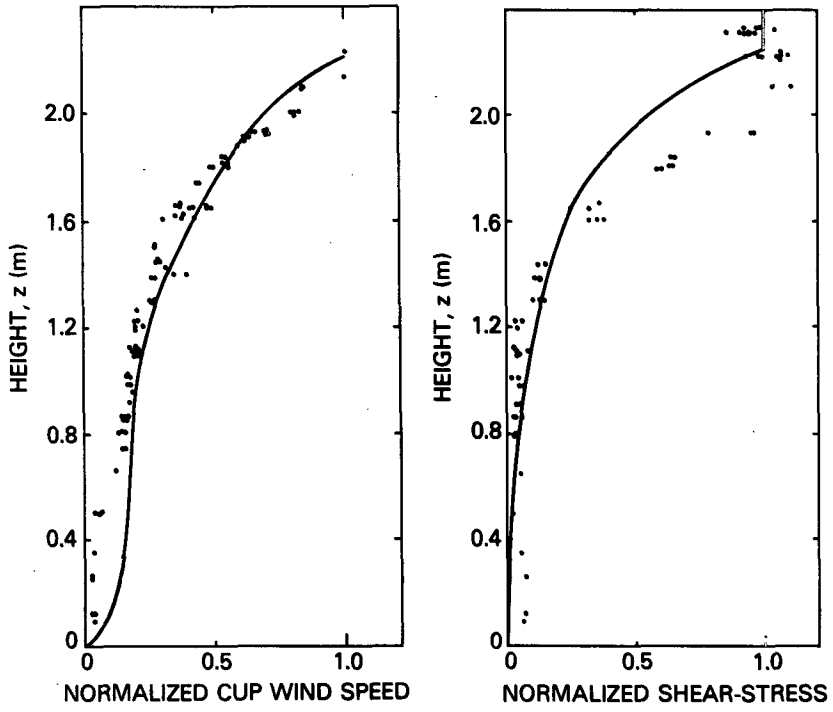

FIG. 3. Profiles of (a) wind speed and (b) shear stress in a maize crop. Points are observations from Wilson et al. (1982) and solid lines are derived from momentum balance equations.

the coefficients describing the wind and stress profiles. To do this, it was necessary to assume that the leaves were distributed more or less uniformly with height and to estimate a roughness length for the soil surface (0.005 m) and a height for the base of the canopy (0.2 m). The predicted profiles provide a reasonable match with the observations in the upper part of the canopy, and the derived values of z_0/z_2, 0.08, and d/z_2, 0.80, are within the range of values reported for a maize crop by Uchijima (1976). Observations and estimates of the vegetation properties at the sites used for the energy and momentum balance studies are listed in Table 2. The relevant morphological data were used to solve the equation set describing transfer conditions above and within the canopy leading to the calculation of values of z_0 and d for each crop.

Figures 5, 6 and 7 in Sellers et al. (1986) illustrate the predicted relationship between z_0, d and the bulk canopy drag coefficient, C_D, taken to be the product of the effective drag coefficient of each canopy element, C_d/p_s, and the leaf area index, $L_t = L_d(z_2 \rightarrow z_1)$. When the canopy drag coefficient is small, the model predicts low values of z_0 and d, corresponding roughly to those for a bare soil surface. As additional material is added to the canopy volume, the values of d and z_0 both increase in a semilinear fashion, with z_0 reaching a peak when the canopy drag coefficient is roughly 0.3 to 0.4. Thereafter, d continues to increase as the moment height of momentum absorption rises with increasing vegetation density: denser, less penetrable canopies present less porous and hence "smoother" surfaces to the atmospheric air flow. This same process makes z_0 decrease with increasing canopy density. The results shown in Figs. 5, 6 and 7 of Sellers et al. (1986) are consistent with those obtained by Shaw and Pereira (1982) which were obtained using a second-order closure model. Of particular interest is the variation in z_0 and d with the assumed values of G_1 and G_2. These parameters describe the departure of the wind profile just above the canopy from the predicted log-linear relationship; essentially they provide the adjustment to the profile which would be made up by the turbulent transport term in a second-order closure model (which is a function of the complete wind and stress profiles). The specification of these parameters is rather arbitrary and has been taken from data. However, it seems that the choice of $G_1 = 2.0$ and $G_2 = 0.5$ provides the best match to data and to the calculations of Shaw and Pereira (1982).

Table 3a lists the values of z_0, d, C_1 and C_2 (the neutral $\overline{r_b}$ and r_d coefficients) as derived for four test sites using the above methods. These estimates, normalized by canopy height in Table 3b, can be compared to the equivalent measurements shown in Table 3c. It would appear that the model yields reasonable values of z_0 and d for the test sites in spite of the use of the simple diffusion description.

[N.B. It should be noted that the estimated values of z_0 and d in SiB are appropriate to the transfer of momentum from the atmosphere to the vegetation and ground. These values of z_0 and d are used in the calculation of r_a, $\overline{r_b}$ and r_d, which govern the transfer of moisture and sensible heat. It can be seen that the derivation of these resistances corresponds to a previous analysis which also investigated the relationship between momentum and heat transfer. Stewart and Thom (1973) proposed that estimates of r_a used for describing vapor transfer from canopies be obtained by

$$r_{a_v} = \frac{\phi_v}{\phi_m} r_{a_m} + r_B$$

where

r_{a_v} vapor transfer resistance, s m^{-1}
r_{a_m} momentum transfer resistance, s m^{-1}
ϕ_v/ϕ_m correction term for diffusion of water vapor and non-neutrality
r_B excess resistance, s m^{-1}.

Note r_B is the additional aerodynamic resistance imposed on heat and water vapor transfer owing to the difference between the modes of momentum and heat/vapor transfer. Stewart and Thom (1973) suggested that r_B could be divided into two parts, i.e.,

r_B = (a bluff body term) + (source/sink term).

Within the SiB model, the bluff body term in r_B is accounted for by the difference between C_d and C_s in $\overline{r_b}$. The source/sink term is a function of the difference between h_a and $z_0 + d$ and is usually small.]

TABLE 3. (a) Momentum, mass and heat exchange properties derived for the test crops. Data from Table 2 were used to solve momentum balance equations (see text and Sellers et al., 1986). Comparison of calculated (b) and observed (c) values of z_0 and d. The observed values are taken from Monteith (1973) for barley, Legg and Long (1975) for wheat, Uchijima (1976) for maize, and Jarvis et al. (1976) for spruce.

	Barley	Wheat	Maize	Spruce
(a)				
z_0 (m)	0.125	0.106	0.161	0.86
d (m)	0.667	0.542	0.774	8.62
$C_1(r_b)$	9.3	7.05	15.1	1.6
$C_2(r_d)$	278.0	232.5	131.0	2450.
(b)				
z_0/z_2	0.123	0.133	0.134	0.086
d/z_2	0.637	0.678	0.645	0.862
(c)				
z_0/z_2	0.06	0.14	0.05–0.15	0.07–0.26
d/z_2	—	0.56	0.53–0.8	0.68–0.84

3) SURFACE RESISTANCE SUBMODEL

The surface resistances $\overline{r_c}$, r_g and r_{surf} control the flux of water vapor from the canopy, ground cover and bare soil surface, respectively, under dry conditions.

Here $\bar{r}_c$ may be thought of as equivalent to all the stomatal resistances of the individual leaves in the canopy acting in parallel (Sellers et al., 1986; Sellers, 1985). Accordingly, it is calculated as the total effect of the stomatal resistance, r_s, of all the leaves in the canopy integrated over all leaf azimuths, ξ, leaf inclinations, θ, and from the top to the bottom of the canopy, that is, over the total leaf area index, L_t. This calculation allows for the effects of differential illumination of individual leaves due to their particular angle to the incoming photosynthetically active radiation (PAR) flux and their position in the canopy. The bulk canopy resistance, as a function of the more influential environmental variables, may therefore be written as

$$\frac{1}{\bar{r}_c} = V_c N_c f(T) f(\delta e) f(\psi_l) \times \int_0^{L_t} \int_0^{\pi/2} \int_0^{2\pi} \frac{O(\xi, \theta)}{r_s(F_\pi, \xi, \theta)} \sin\theta \, d\xi \, d\theta \, dL \quad (20)$$

where

L	leaf area index
V_c	upper-story cover fraction
N_c	fraction of upper-story canopy that consists of live, photosynthetically active leaves
$O(\xi, \theta)$	leaf azimuth, inclination distribution function
ξ, θ	leaf azimuth, inclination angles
$f(T), f(\delta e), f(\psi_l)$	stomatal resistance adjustment factors for the effects of leaf temperature, T, vapor pressure deficit, δe, and leaf water potential, ψ_l, respectively. All three factors vary between 1 (optimal conditions) and zero (full stomatal closure).

Note that r_s is the stomatal resistance of an individual leaf, in s m^{-1}, and is given by

$$r_s = \frac{a}{b + \mathbf{F}_\pi \cdot \mathbf{n}} + c \quad (21)$$

where

$\mathbf{F}_\pi$	photosynthetically active radiation flux, W m^{-2}
$\mathbf{n}$	vector of leaf normal
a, b, c	species dependent constants; J m^{-3}, W m^{-2}, s m^{-1}.

A discussion of the dependence of $\bar{r}_c$ on different leaf angle distributions is presented in Sellers (1985). For the purposes of the tests discussed in this paper, we shall use the average leaf projection as a function of μ, $\overline{G(\mu)}$, proposed by Goudriaan (1977) based on the work of Ross (1975), to replace the leaf angle distribution function $O(\xi, \theta)$. Use of an average leaf projection for a given PAR flux direction greatly simplifies the solution of (20), as the angular integrations may be dropped. This simplification does not produce markedly different results from those obtained with a solution including the full angular terms, $d\xi$ and $d\theta$.

The Ross–Goudriaan function (Goudriaan, 1977) is given by

$$G(\mu) = \phi_1 + \phi_2 \mu \quad (22)$$

where

$G(\mu)$	mean projection of leaves in direction μ
ϕ_1, ϕ_2	coefficients from Goudriaan (1977) (see Sellers et al., 1986), taken as functions of χ_L
χ_L	leaf angle distribution factor.

The use of (22) in (20), where it replaces the $O(\xi, \theta) \times \sin\theta$ term, reduces (20) to

$$\frac{1}{\bar{r}_c} = V_c N_c f(T) f(\delta e) f(\psi_l) \int_0^{L_t} \frac{\overline{G(\mu)}}{r_s} dL. \quad (23)$$

The values of the constants used in (20), (21) and (22) are listed in Table 2 for the test crops. Figure 4 shows the data and lines of best fit used to obtain the constants for the PAR-dependent part of r_s (see Eq. 21) for the test crops, that is, a, b and c. It is clear that there is quite a large amount of scatter in the data leading to some uncertainty in the values of these coefficients; the effect of this uncertainty on the estimation of fluxes is discussed in later sections.

In SiB, the bulked form of (23) is used in preference to the fully integrated form of (20). This necessitates the specification of a single direction for the incoming PAR flux which in reality is made up of both diffuse and direct components. A mean angle of PAR incidence is estimated by considering the flux-weighted angles of the direct and diffuse contributions to the total PAR flux.

The behavior of (20) and (23) has been explored in some detail and the results published in Sellers (1985). The main findings of this work were as follows:

(i) Additional increments in leaf area index have diminishing contributions to the value of $1/\bar{r}_c$. This is because denser canopies have a higher proportion of shaded leaves with partially closed stomata.

(ii) The effects of different leaf angle distributions on the value of $1/\bar{r}_c$ are small except for canopies consisting of near-vertical leaves. Most canopies exhibit intermediate leaf angle distributions.

(iii) As a result of (ii) above, the simplified $1/\bar{r}_c$ expression, (23), which uses the Ross–Goudriaan function yields results which compare closely with those provided by the more exact formulation of (20).

The value of $\bar{r}_c$ estimated from the integral parts of (20) and (23) relates only to the PAR dependence of stomatal control, and so represents the minimum attainable value of $\bar{r}_c$. The factors outside the integral represent the effects of nonoptimal temperature, vapor pressure deficit and leaf water potential conditions, the form of which were taken from Jarvis (1976) and reproduced in Sellers et al. (1986). The parameters involved in each are now briefly discussed.

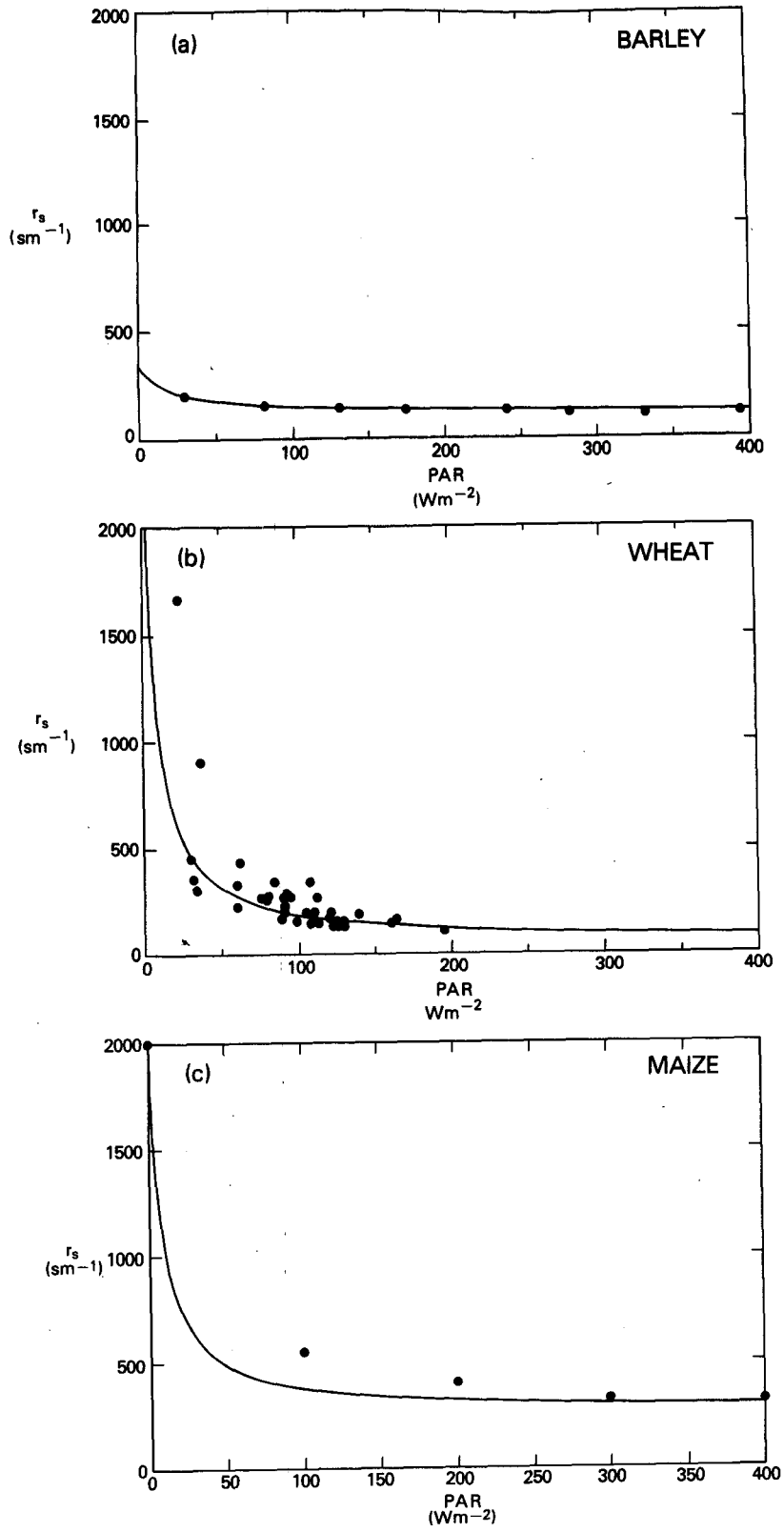

FIG. 4. Relation between stomatal resistance, r_s, and incident visible or PAR flux for (a) barley, (b) wheat, (c) maize and (d) Sitka spruce leaves. Data are from Monteith et al. (1965), Denmead and Millar (1976), Turner (1974) and Jarvis (1976), respectively. Solid lines represent best fit curves for equation (21) in text. [Visible flux is estimated from the total shortwave flux in original dataset in (a) and 0.625 of the net radiation absorbed by the leaf in (b).]

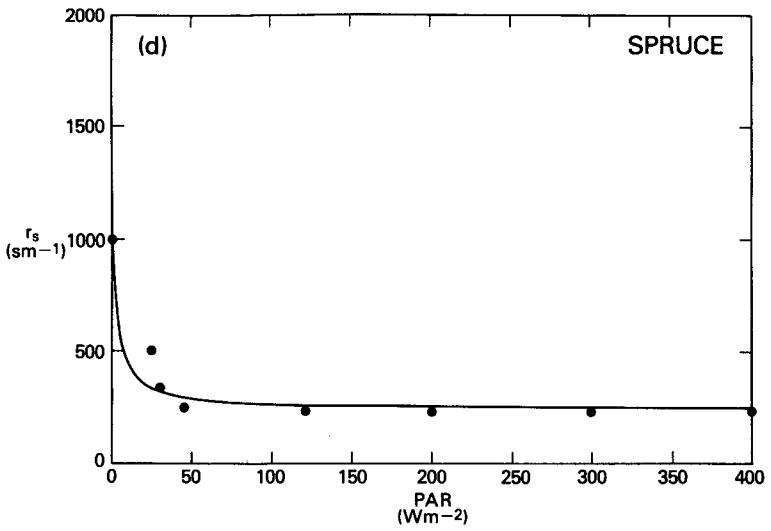

FIG. 4. (*Continued*)

The temperature dependence function, $f(T)$, requires the specification of cutoff points: the minimum and maximum temperatures at which photosynthesis and hence transpiration can occur [$f(T) = 0$]; and an optimal temperature, [$f(T) = 1$]. The vapor pressure deficit function specifies a linear decline in $f(\delta e)$ against an increase in the vapor pressure deficit, $\delta e = e^*(T_a) - e_a$. Probably the most important factor governing $\bar{r}_c$, besides incident radiation, is $f(\psi_l)$ which accounts for the effect of leaf water potential on r_s. For these tests and for operational use in SiB, the original expression for $f(\psi_l)$ proposed by Jarvis (1976) has been replaced by a linear function which is more manageable from the modeling viewpoint, namely,

$$f(\psi_l) = \frac{\psi_l - \psi_{c_2}}{\psi_{c_1} - \psi_{c_2}}, \quad 0 \leq f(\psi_l) \leq 1 \tag{24}$$

where

ψ_{c_1} leaf water potential at which stomata start to close, m

ψ_{c_2} leaf water potential at which stomata are completely closed, m.

When the vegetation's water potential is greater than ψ_{c_1}, i.e., no leaf water potential stress, $f(\psi_l) = 1$.

Jarvis's $f(\psi_l)$ formulation involves an exponential term which necessitates the inclusion of an iterative solution technique when calculating the transpiration flux as a function of evaporative demand, soil moisture potential and plant characteristics. Use of (24) allows one to specify the same nonlinear problem as a quadratic equation, as first proposed by Choudhury (1983), with considerable advantages in computational reliability and efficiency. It has been found that the simulation results are insensitive to the exact form of the $f(\psi_l)$ relationship so all current versions of SiB therefore make use of (24).

There are few data against which to check the validity of the $\bar{r}_c$ formulation in SiB. Figure 5 shows the data of Monteith et al. (1965) in which r_s (for leaves near the top of the canopy) and the surface resistance, taken to be equivalent to $\bar{r}_c$, were measured for a barley crop via a diffusion porometer and the energy balance method, respectively. Also shown is the fit of (21) to the r_s values and the predicted course of $\bar{r}_c$ for two leaf area indices as given by (20). We should expect the value of $\bar{r}_c$ given by (20) to be an underestimate as no allowance has been made for the effects of leaf water potential, leaf temperature and leaf age. (The r_s measurements were taken on young green leaves while those at the canopy base were senescent.) The results in Fig. 5 illustrate how additional increments in leaf area index have diminishing effects on the surface resistance. This is because the leaves at the base of the canopy are shaded and have correspondingly narrower stomatal apertures.

The effects of changing the parameters in the adjustment factors $f(T)$, $f(\delta e)$, $f(\psi_l)$ are discussed in ensuing sections. Generally speaking, most vegetation types have temperature optima, $f(T_0) = 1$, close to the mean temperature found in their environments and cutoff points around the freezing point of water (273 K) and at 45°C (318 K). Response to leaf water potential varies more from species to species, but most plants are unaffected until ψ_l drops below −100 m, and few plants continue to photosynthesize or transpire beyond $\psi_l = -500$ m. The feed-forward closure response of stomata to increasing vapor pressure deficits, $\delta e = [e^*(T_a) - e_a]$, has been most frequently observed in coniferous species.

The data used for calculating soil, root and stem resistances are listed in Table 2.

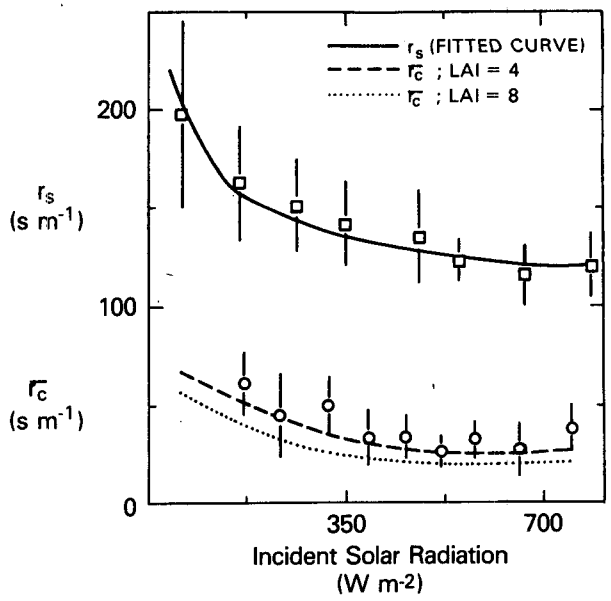

FIG. 5. Data showing variation of r_s (top leaves) and $\bar{r}_c$ for a barley crop with incident solar radiation from Monteith et al. (1965). PAR is estimated to be half of the global incident flux. Lines show fit to r_s (as in Fig. 4) and estimate of r_c as given by Eq. (20) in text for leaf area indices of 4.0 and 8.0.

c. *Complete model performance*

The three submodels have been tested separately and have been shown to operate consistently and realistically. Next, we move on to the evaluation of the performance of the complete SiB model using the data collected at the test sites (see section 3.1). In all the simulation runs described in this section, the canopy and ground temperatures, T_c and T_{gs}, were initialized with the first air temperature observation; the interception stores, M_c and M_g, were assumed to be zero; and the soil moisture contents were initialized from observations. Thereafter, all these variables were advanced prognostically as the simulation progressed.

1) SITE A: BARLEY AND WHEAT

The downward longwave radiation measurements taken on the bare soil plot were found to be erroneous (values ranged from -20 to $+600$ W m^{-2}). An estimate of this quantity was provided by subtracting the calculated absorbed shortwave radiation and surface-emitted longwave radiation, a function of T_c and T_{gs}, from the measured net radiation, yielding the downward longwave flux as a residual. This procedure is carried out at the beginning of each time step and so the estimate of longwave flux is effectively one time step behind the energy balance calculation; however, as the downward longwave flux does not vary rapidly and the simulation time step is relatively short (1 h), the results should be acceptable.

Figure 6a shows the simulated and measured courses of net radiation, latent heat flux and sensible heat flux for the barley I plot. Because of the way the energy balance is closed by the calculation of the downward longwave flux, the calculated net radiation is constrained to be a close match to the observations. The predicted partitioning of energy into sensible and latent heat fluxes is in general agreement with the observations both in terms of magnitude and diurnal variation. Figure 6b shows a direct comparison of the observed and predicted latent heat fluxes for the barley I plot, corresponding to results shown in Fig. 6a. The model may slightly overestimate evapotranspiration rates, particularly when the atmospheric demand is high, due to a slight underestimation of the canopy resistance term, $\bar{r}_c$, which was estimated from the original data of Monteith et al. (1965); see Fig. 5.

Figure 7 shows the predicted course of surface temperature, T_s, for the barley II plot for a range of assumed surface emissivities. (Surface temperature was estimated from a weighted combination of T_c^4 and T_{gs}^4, the weights being determined by the fractions of canopy and ground that were calculated to be visible from a vertical view-angle.) Also shown are some measurements of surface temperature taken with a hand held radiometer. Little can be learned from this comparison of simulation with data in view of the unreliability of the data and the uncertainties in the surface emissivity and other quantities except that the diurnal pattern and amplitude of the observations are approximately reproduced in the simulation.

Figure 8 shows the predicted variation in $\bar{r}_c$, ψ_l and $f(\psi_l)$ for the barley II plot for the period of 20 to 21 June 1979. Also shown are a number of measured r_s values (as obtained by a diffusion porometer; see van der Ploeg et al., 1980) normalized by the leaf area index to allow comparison with the predicted values of $\bar{r}_c$. The solid circles on the 20 June observations correspond to an estimated effective $\bar{r}_s$ as derived from the inverse sum of the r_s measurements for individual leaves. The minimum and maximum $\bar{r}_s$ values correspond to the observations for leaves at the top and bottom of the canopy, respectively. The relation between the mean and minimum values of $\bar{r}_s$ on 20 June was used to estimate the mean value of $\bar{r}_s$ from observations of r_s for the leaves at the canopy top (which were all that were recorded on 21 June) via a regression equation. The estimated values of mean $\bar{r}_s$ on 21 June should therefore be used only as a guide to the diurnal trend.

The light-limited value of $\bar{r}_c$, as given by the integral part of (23), is shown by the lower line in Fig. 8a. The final value of $\bar{r}_c$ used by the model, i.e., the light-limited value multiplied by the adjustment factors, is shown by the upper line which should be compared to the $\bar{r}_s$ data points.

The magnitudes and diurnal trends of the predicted values of $\bar{r}_c$ are in general agreement with the observations except for the afternoon of 21 June. In general,

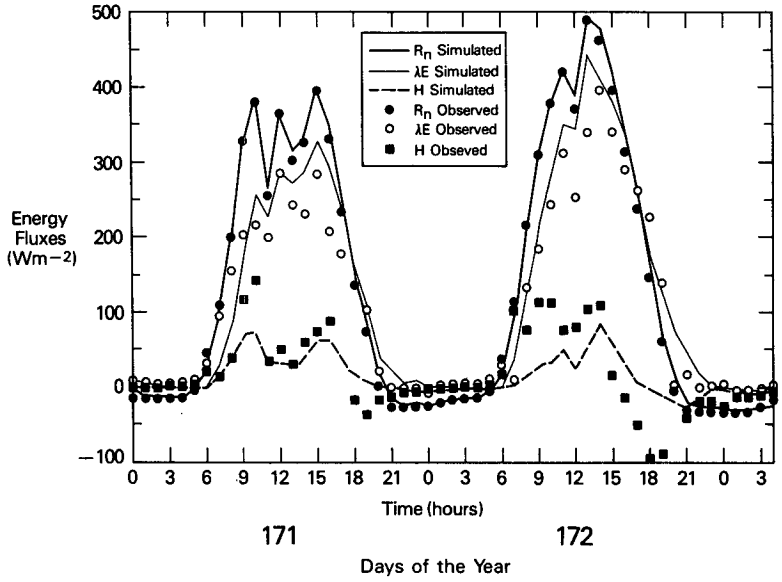

FIG. 6a. Observed and predicted values of net radiation, R_n, latent heat flux, λE, and sensible heat flux, H, for the barley I plot, Ruthe, W. Germany for 20–21 June 1979.

$\bar{r}_c$ approaches its light-limited value in the morning and then increases during the day as the evaporative demand rises and the leaf water potential falls. This trend is particularly clear on 20 June where the $\bar{r}_s$ data are more reliable (three measurements of $\bar{r}_s$ over the height of the canopy at each sampling time).

Table 4 shows the simulated and observed daily totals of the energy fluxes for the barley I and wheat III plots using the parameters listed in Table 2. It would appear that the model calculates the partitioning of energy for the barley site in a reasonable way.

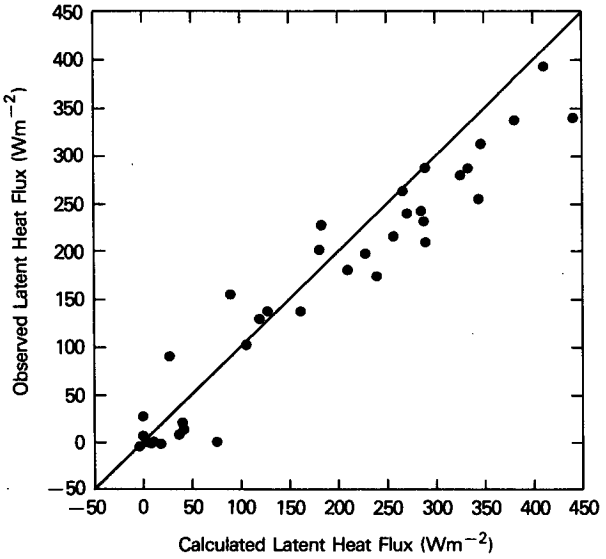

FIG. 6b. Comparison of observed and predicted values of latent heat flux for the barley I plot, Ruthe, W. Germany for 20–21 June 1979.

No local flux observations were available for comparison with the wheat simulations, so data from a study conducted at Volkenrude, some 50 km distant from the Ruthe site, are shown for comparison in Table 4. The disparity between the simulated and observed net radiation values may be atrributed to differences in cloudiness between the two sites and are reflected in the corresponding evapotranspiration rates on 20 June. The observations for 21 June should be regarded with some suspicion as the sensible heat flux was reported to be strongly negative (~ -90 W m^{-2}) in the early evening and positive (away from the surface) at night. The predicted ratio of evapotranspiration to net radiation for the wheat crop corresponds to the observed ratio for the nearby barley site which also suggests that the observations were suspect on this day. In summary, the models appear to perform plausibly in the simulation of the diurnal energy balance and the calculation of total fluxes. Where reliable data are available, the subcomponents of the model (radiation interception, stomatal resistance, etc.) seem to operate realistically.

2) SITE B: MAIZE

The tests with the maize data sets were used to investigate the relationship between ψ_l, $\bar{r}_c$ and evaporative demand. Figure 9 shows the observed and predicted time course of leaf water potential for the maize crop for 2 days and the simulated $\bar{r}_c$ values with and without the adjustment for leaf water potential. The model ap-

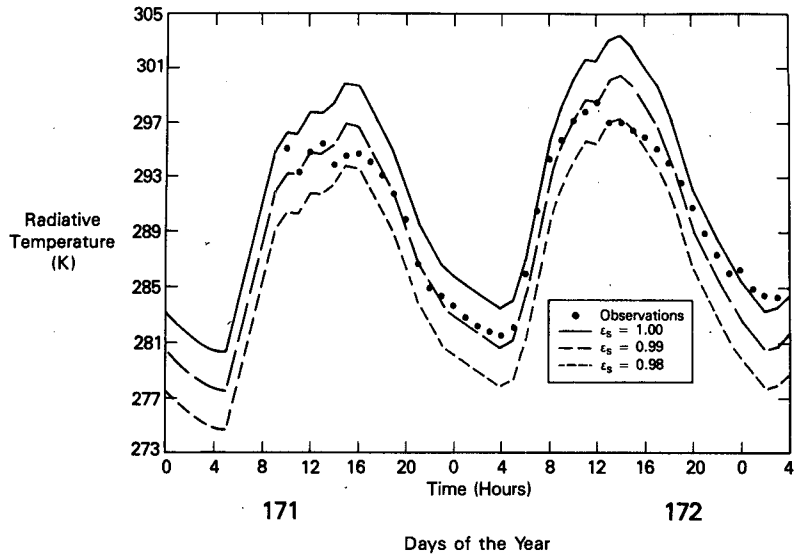

FIG. 7. Predicted course of apparent surface temperature for the barley II plot, Ruthe, W. Germany for 20–21 June 1979 using three different surface emissivity (ϵ_s) values. The data points represent observations made using a hand-held radiometer.

pears to perform realistically except for failing to predict the dip in the ψ_l observations on the afternoon of day 167. Choudhury (personal communication) has speculated that this feature may be due to the plants' internal water storage reserve becoming depleted by the late afternoon but there is, as yet, no data to test this hypothesis. Since SiB does not consider the plants' internal water storage capacity within the transpiration calculation, this phenomenon cannot be modeled with the existing formulation.

3) SITE C: NORWAY SPRUCE

The micrometeorological forcing data for the Norway spruce site were recorded in a clearing some short distance away from the forest and were adjusted by comparisons with occasional sets of observations recorded with an automatic weather station (AWS) above the canopy. It was assumed that the adjusted values were representative of conditions at the height of the second AWS, i.e., roughly 2 m above the canopy. The

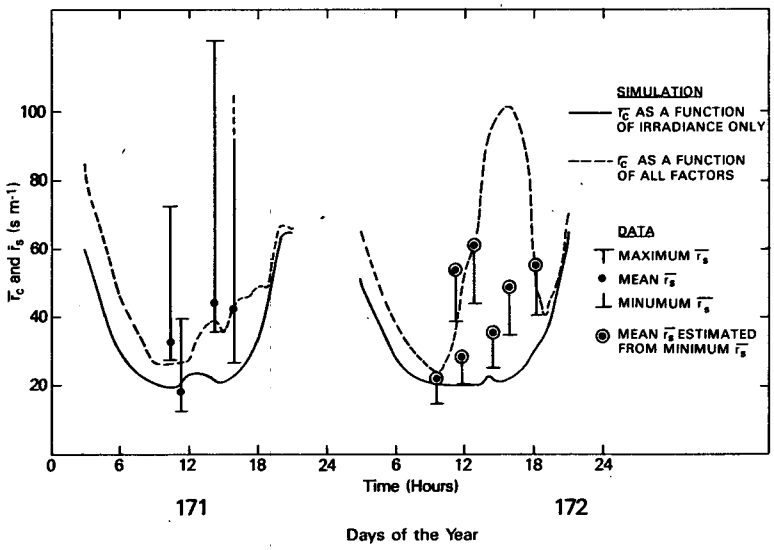

FIG. 8a. Predicted ($\bar{r}_c$) and estimated ($\bar{r}_s$) values of the bulk stomatal resistance for the barley crop at Ruthe, W. Germany, 20–21 June 1979. See text for method of deriving $\bar{r}_s$ values from individual measurements of r_s.

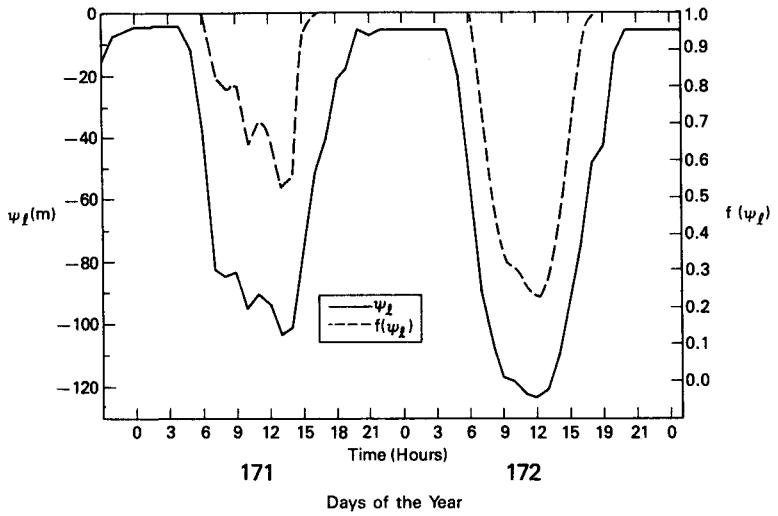

FIG. 8b. Predicted leaf water potentials, ψ_l, and adjustment factor, $f(\psi_l)$, for the barley I plot, Ruthe, W. Germany, 20–21 June 1979.

shortwave radiation flux was partitioned into the four components required by the SiB model using the scheme of Goudriaan (1977). Once again, no downward longwave radiation fluxes were measured, so these were estimated as residuals in the same way as was done for wheat and barley. Finally, the lowest soil moisture store was assumed to drain at a rate determined by gravity and the sine of the local slope angle, taken to be 10°. (Since the forest's transpiration rate was never at any time thought to be limited by low leaf water potentials, the exact level of the soil moisture store was not critical to this simulation.) Figure 10 shows the performance of the SiB simulation in calculating interception loss rates and combined transpiration/soil evaporation rates over a 40-day period in 1975. While nothing can be said about the realism of the diurnal pattern of energy partition, it is clear that the model predictions follow the long-term running total fairly closely. Differences between the observed and predicted transpiration losses can be assigned to uncertainties in the parameters governing stomatal control (see later sections).

Figure 11 shows a 3-day simulation of the energy balance for the forest together with the associated canopy resistance. Calder (1978) estimated the mean canopy resistance for the site to be about 75 s m^{-1} with a seasonal variation of some 25 s m^{-1}. This is in broad agreement with the values calculated by SiB over the

TABLE 4. Observed and calculated time-averaged (~) values of net radiation, R_n, soil heat flux, G, sensible heat flux, H, and latent heat flux, λE, all in $W\ m^{-2}$. The calculated contributions of soil evaporation and transpiration to the latent heat flux are also shown. The asterisk denotes that data were recorded at Volkenrude, 50 km away from Ruthe. All other values refer to Ruthe, Federal Republic of Germany.

	$\tilde{R}_n$	$\tilde{G}$	$\tilde{H}$	$\lambda\tilde{E}$	Transpiration	Soil Evaporation
			20 June: Barley			
Simulated	143.3	2.7	22.1	118.5	98.6	19.9
Observed	137.6	−4.1	25.5	108.0	—	—
			21 June: Barley			
Simulated	162.9	−0.01	12.1	150.7	121.3	29.4
Observed	155.6	−6.9	15.6	133.1	—	—
			20 June: Wheat			
Simulated	166.2	1.8	43.3	121.9	98.2	23.7
Observed*	132.8	−4.4	18.4	110.1	—	—
			21 June: Wheat			
Simulated	161.1	0.14	29.1	133.0	102.2	30.8
Observed*	163.7	−5.8	−31.9	189.9	—	—

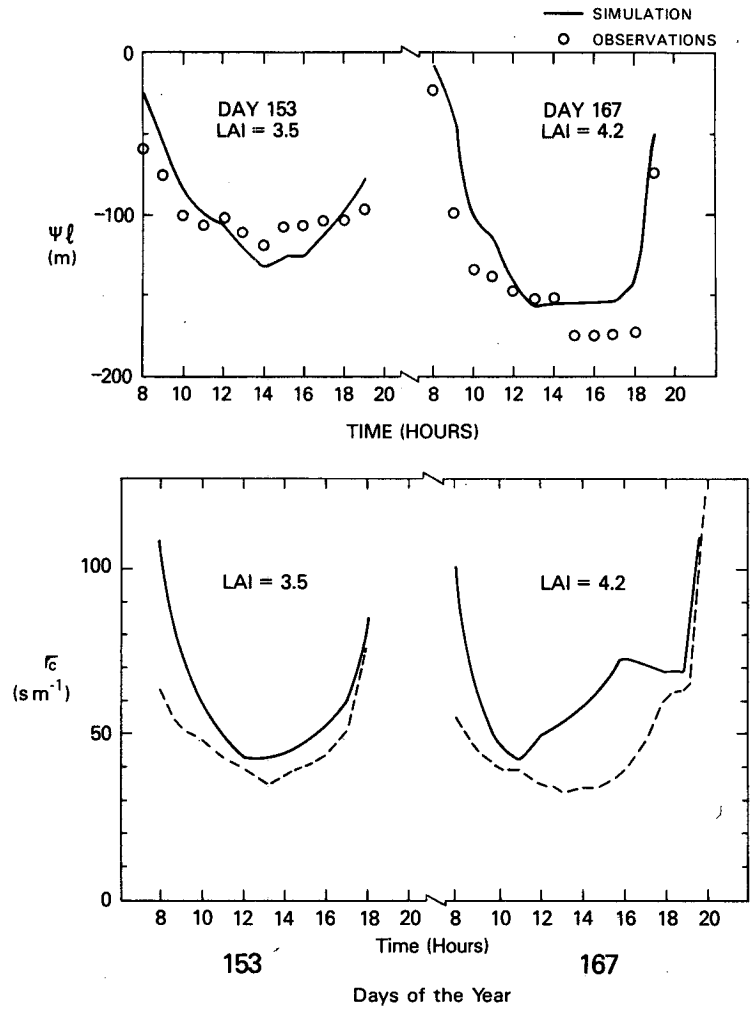

FIG. 9. Observed and predicted time course of (a) leaf water potential ψ_l, and (b) canopy resistance, $\bar{r}_c$, for a maize crop over 2 days. The lower values of $\bar{r}_c$ correspond to the light-limited estimate while the higher ones include the effects of leaf water potential and leaf temperature; see Eqs. (20) and (23) in the text.

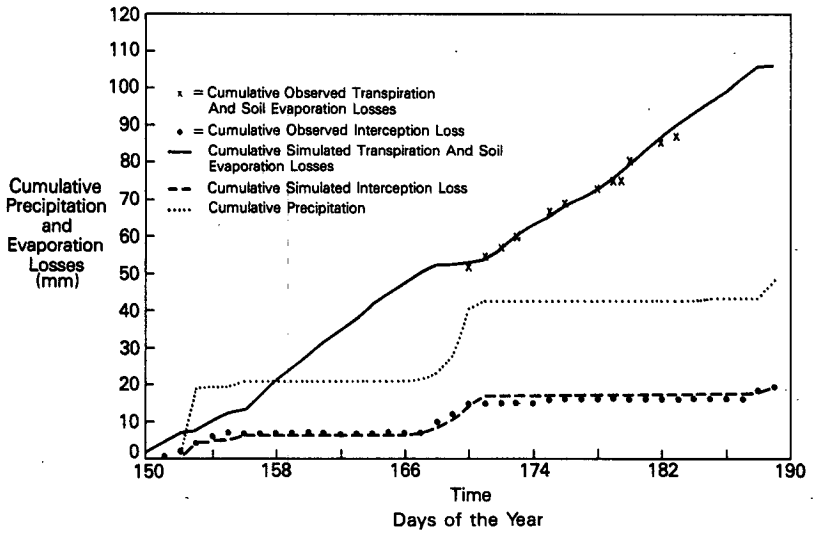

FIG. 10. Results of 40-day simulation for the spruce site, Plynlimon, Wales, compared with observations. Soil evaporation and canopy transpiration are combined to give a single cumulative total flux. Cumulative totals of precipitation and interception loss are also shown.

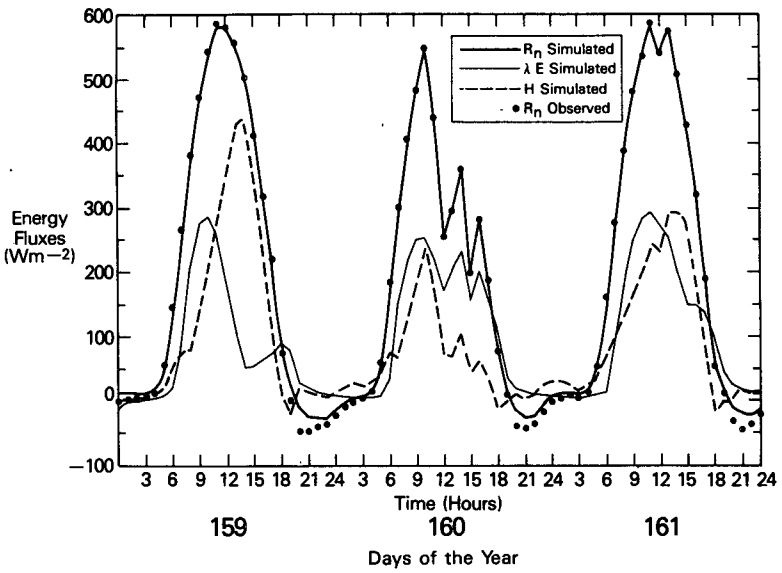

FIG. 11a. Predicted values of net radiation, R_n, latent heat flux, λE and sensible heat flux, H, for the spruce site for three sunny days.

midday hours. The effects of the vapor pressure deficit factor, $f(\delta e)$, may be seen clearly in Fig. 11 as this term is the dominant one in determining the departure of $\bar{r}_c$ from its light-limited value.

Figure 12 shows the simulated energy balance for the spruce forest for three rainy days. Sometimes the latent heat flux is calculated to exceed the net radiation, inducing large negative sensible heat fluxes. The maintenance of such a large vertical advection of energy is made possible by the low aerodynamic resistance generally associated with tall vegetation (Hancock et al., 1983).

4. Sensitivity of model simulations to variations in the input parameters and initialization

a. Methodology of sensitivity trials

In specifying the design of the Simple Biosphere model, Sellers et al. (1986) attempted to represent the various components of the soil–plant–atmosphere system in as realistic a way as possible given the constraints of operating within the computing environment of atmospheric general circulation models. As a result, the model has a large number of input parameters (see Table 1 of Sellers et al., 1986) all of which must be

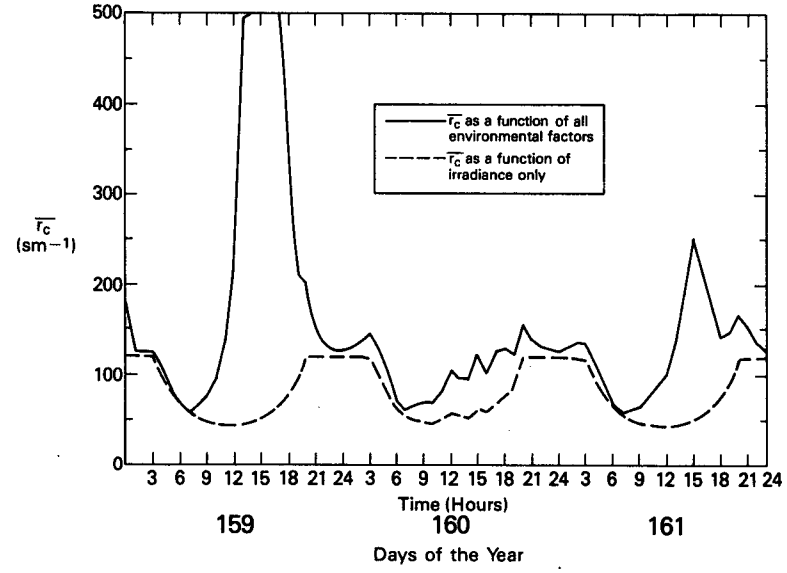

FIG. 11b. Predicted variation in $\bar{r}_c$ for the spruce site for three sunny days. Lower line refers to light-limited value of $\bar{r}_c$, upper line to final estimate of $\bar{r}_c$.

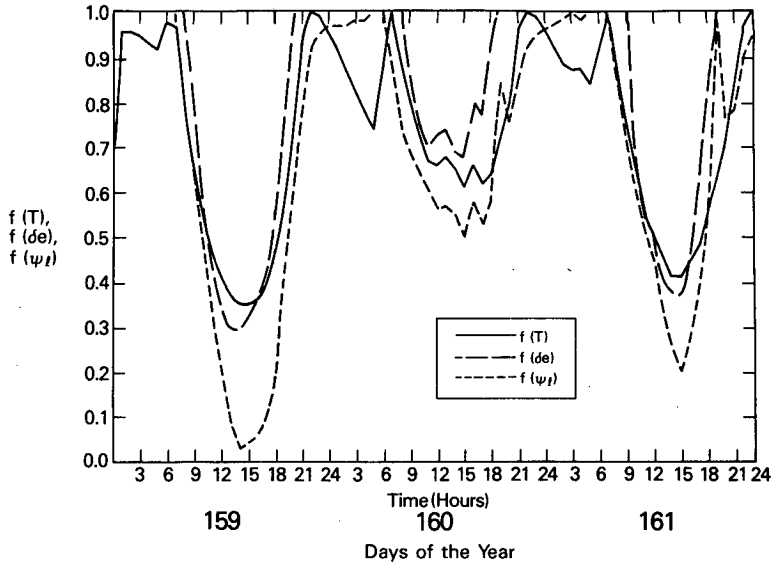

FIG. 11c. Predicted values of $f(\delta e)$, $f(T)$ and $f(\psi_l)$ for the spruce site for three sunny days.

specified in order to run the model. While it is true that most of these parameters correspond directly to physically measurable quantities, it is also true that some of them will be subject to a large degree of uncertainty for the following reasons:

(a) Measurements of many of the parameters are scarce for different biomes in different parts of the world. A wide degree of scatter is often associated with the data that do exist.

(b) The GCM grid areas are commonly of the order

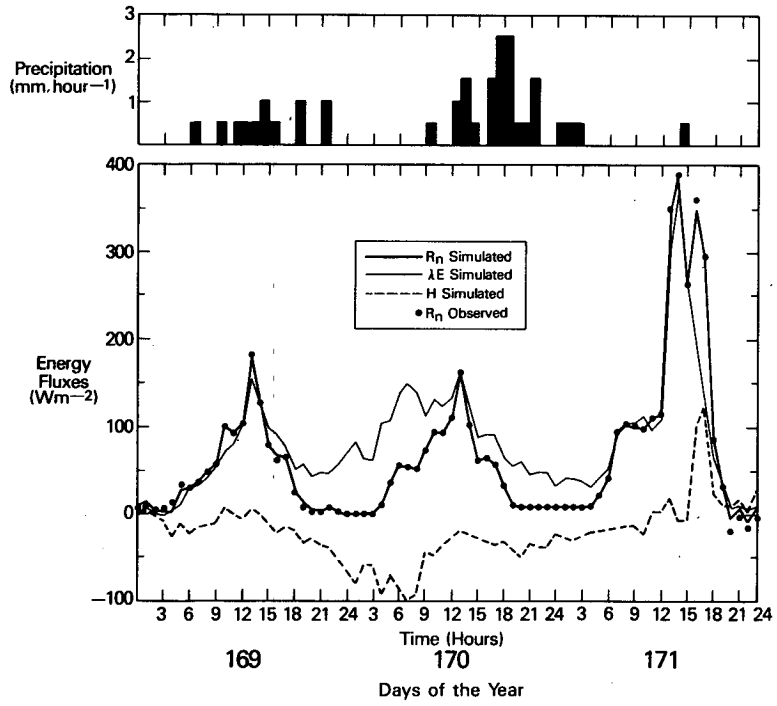

FIG. 12. Predicted values of net radiation, R_n, latent heat flux, λE, and sensible heat flux, H, for three rainy days. Precipitation rates are shown at the top of the figure.

of (100 km)^2 to (400+ km)^2 in size. Even if we assume that a grid area is more or less completely covered by one particular biome, the variability of the form and physiological responses of the vegetation will vary considerably. For example, it would be practically impossible to specify the mean height of a mature tropical rain forest canopy to within a factor of better than ±25%.

Both of the above causes of uncertainty have to be addressed if the SiB model's representation of global vegetation is to be meaningful within the context of GCM experiments. This section explores the effects of the uncertainties in the input parameters on the important quantities returned to the atmospheric part of the GCM, i.e., momentum, heat and vapor fluxes, reflected shortwave radiation and the upward flux of thermal radiation (a function of T_c and T_{gs}). In all of the following discussion, we have tended to be conservative in making the errors or uncertainties of the input parameters larger than we would hope our true dataset would reflect. The resultant sensitivity analysis also allows us to be selective in the effort we put into searching for accurate data to put into the GCM version of SiB because those parameters which are found to have little influence on the model output need only be coarsely quantified.

The discussion is arranged to cover the three submodels of the SiB model in turn. Additionally, the sensitivity of the model calculations to variations in the initialization of the prognostic variables is discussed. (It is clear that in this respect the only prognostic variables that have a significant effect on the model performance are those associated with soil moisture content.) In each case, we shall use the examples of the barley crop and Norway spruce forest already described in this paper as the bases for the sensitivity analysis. These two vegetation types have marked differences in morphology and physiology and so between them provide us with a reasonably respresentative framework for the discussion. In all of the discussion that follows, we have adopted a standard methodology for the analysis which may be summarized as follows:

(i) Selection of the time period for the analysis (all the data, 2 days, for barley; and two 3-day periods for spruce to represent wet and dry conditions).

(ii) Running the SiB model on the selected meteorological data using the original vegetation input parameters sets (see previous sections) to produce "standard" runs. These runs also calculate time series of the downward longwave radiation flux which are used as input for the sensitivity runs.

(iii) Sequential adjustment of the input parameters and rerunning of the model to investigate sensitivity of the time-averaged (denoted by wavy overbars) fluxes of net radiation, $\tilde{R}_n$, ground heat flux, $\tilde{G}$, latent heat flux, $\lambda\tilde{E}$ and sensible heat flux, $\tilde{H}$. Sometimes a distinction is made between the separate contributions of interception loss, $\lambda\tilde{E}_{\omega}$, and transpiration loss, $\lambda\tilde{E}_d$, to the latent heat flux, $\lambda\tilde{E}$. For these runs, all the radiative forcing is provided by the input data; the downward longwave flux is taken from the output of the "standard" runs.

b. *Radiative transfer*

The functioning and sensitivity of the radiative transfer submodel in SiB has been discussed exhaustively in Sellers (1985). The effects of solar angle, leaf angle distribution, soil surface reflectance, etc., were described comprehensively with reference to the radiative transfer model output. It remains at this stage to examine the effects of uncertainties in the values of the leaf scattering coefficient, ω, which is made up of the sum of the leaf transmittance and reflectance. Table 5 shows the effects on the energy fluxes of reducing and increasing the value of the leaf scattering coefficient by 10%. It is clear that a given percentage change in ω leads to smaller percentage change in the surface albedo and hence the net radiation flux $\tilde{R}_n$. This is partly because of the influence of multiple scattering within the canopy, which tends to damp the effects of large changes in ω on the total canopy reflectance. Additionally, when less shortwave radiation is absorbed by the canopy, the resultant cooling of the surface produces a compensating increase in the net longwave radiation flux towards the surface.

The subsequent effects of these changes in the net radiation on the flux terms $\lambda\tilde{E}$ and $\tilde{H}$ may be assessed from the same tables. Under dry conditions, the change in net radiation mainly seems to influence the sensible heat flux term, implying that the latent heat flux is relatively insensitive to changes in net radiation, being more a function of the drying power of the air and the canopy resistance term, $\overline{r_c}$. Under wet conditions, however, the $\overline{r_c}$ term is subordinate and so the changes in net radiation are partitioned more equally between the flux terms H and λE.

Kimes et al. (1987) explored the role of foliage clustering in increasing the effectiveness of the canopy as a radiation trap. It was found that clustering and spatial heterogeneity, both of which are features common to most coniferous canopies, could decrease the albedo of the vegetated surface by a few percent. We have not yet accounted for the effects of foliage clustering on surface reflectance within the SiB radiation model, so the uncertainty generated by this omission has not been definitely quantified.

To summarize, uncertainties in the radiative transfer properties of the vegetation–soil system seem to have proportionately smaller effects on the calculated net radiation. Under dry conditions, the resultant uncertainties in the net radiation flux tend to affect the sensible heat flux calculation most strongly, the evapotranspirative flux being relatively insensitive to the value of R_n. Under wet conditions, changes in R_n seem

TABLE 5. Summary of sensitivity analyses performed on (a) the barley site for two sunny days, (b) the spruce site for three sunny days and (c) the spruce site for three rainy days. In (c), the dependence of the energy fluxes on physiological properties has been omitted due to their insignificance under precipitating conditions. In each case, the second column of figures, labeled with "%," refers to percentage change from the standard run. N.B. λE_ω refers to the sum of canopy interception loss and soil evaporation.

5 (a) Barley, sunny days: 171–172

	R_n		G		λE		H	
	$\tilde{R}_n$	$\%R_n$	$\tilde{G}$	$\%G$	$\lambda\tilde{E}$	$\%\lambda E$	$\tilde{H}$	$\%H$
				Standard				
	153.1	—	1.3	—	134.6	—	17.1	—
				Aerodynamic				
$r_a/2$	152.8	−0.2	1.4	+4.6	134.2	−0.3	17.3	+2.8
r_a^*2	149.8	−2.1	1.4	+5.4	128.9	−4.2	19.5	+13.7
$\overline{r_b}/2$, $r_d/2$	153.9	+0.5	1.1	−17.5	142.8	+6.1	9.9	−42.0
$\overline{r_b}^*2$, r_d^*2	150.0	−2.0	1.7	+28.3	124.5	−7.5	23.8	+38.6
				Radiation				
$\omega/1.1$	161.4	+5.4	1.4	−4.3	136.9	+1.7	23.1	+34.6
$\omega^*1.1$	140.3	−8.4	1.5	+15.4	128.2	−4.8	10.5	−38.7
				Biophysical				
$r_c^*0.75$	153.6	+0.3	1.4	+4.1	138.0	+2.5	14.2	−17.3
$r_c^*1.25$	152.0	−0.7	1.5	+9.3	129.8	−3.5	20.7	+20.8
$L_t/2$	153.7	+0.4	1.4	+5.7	134.9	+0.3	17.3	+0.9
$L_t^*1.5$	153.1	—	1.4	+8.2	135.0	+0.3	16.7	−2.6
$r_{pl}/2$	152.8	−0.2	1.5	+9.4	136.1	+1.1	15.2	−11.1
r_{pl}^*2	151.8	−0.9	1.5	+9.1	127.3	−5.4	22.9	+33.6
$r_{root}/2$	153.3	+0.1	1.6	+18.4	142.6	+6.0	9.1	−46.8
r_{root}^*2	147.0	−2.0	1.5	+11.6	111.7	−17.0	36.9	+115.1
				(ψ_{c_1}, ψ_{c_2})				
−85, −160	152.8	−0.2	1.6	+19.1	136.8	+1.6	14.4	−16.0
−100, −180	153.5	+0.3	1.4	+8.4	140.8	+4.6	11.2	−34.4
−115, −200	153.7	+0.4	1.5	+15.6	142.0	+5.6	10.1	−41.3

$\tilde{r}_a$	$\tilde{\overline{r}}_b$	$\tilde{r}_d$	$\tilde{\overline{r}}_c$	$\lambda\tilde{E}_\omega$	$\lambda\tilde{E}_d$
48.9	19.9	950.6	51.2	24.7	109.9

5 (b) Spruce, sunny days: 159–161

	R_n		G		λE		H	
	$\tilde{R}_n$	$\%R_n$	$\tilde{G}$	$\%G$	$\lambda\tilde{E}$	$\%\lambda E$	$\tilde{H}$	$\%H$
				Standard				
	194.1	—	3.3	—	96.4	—	94.3	—
				Aerodynamic				
$r_a/2$	195.4	+0.7	3.3	—	95.4	−1.0	96.7	+2.5
r_a^*2	191.3	−1.4	3.4	+1.0	97.3	+1.0	90.5	−4.0
$\overline{r_b}/2$, $r_d/2$	194.6	+0.3	3.1	−6.0	100.7	+4.4	90.8	−3.8
$\overline{r_b}^*2$, r_d^*2	193.3	−0.4	3.5	+6.0	93.8	−2.7	95.9	+1.7
				Radiation				
$\omega/1.1$	201.6	+3.9	3.3	—	95.8	−0.6	102.4	+8.6
$\omega^*1.1$	183.5	−5.4	3.3	—	97.6	+1.2	82.5	−12.5
				Biophysical				
$r_c^*0.75$	195.1	+0.5	3.3	—	123.4	+28.0	68.3	−27.6
$r_c^*1.25$	193.4	−0.3	3.3	—	78.0	−19.1	112.0	+18.8
$L_t/2$	193.4	−0.4	3.3	−2.1	72.9	−24.4	117.2	+24.3
$L_t^*1.5$	194.7	+0.3	3.4	+4.0	115.0	+19.3	76.2	−19.2
$r_{pl}/2$	194.1	—	3.3	—	96.4	—	94.3	—
r_{pl}^*2	194.1	—	3.3	—	96.1	−0.3	94.5	+0.3
$r_{root}/2$	194.1	—	3.3	—	96.4	—	94.3	—
r_{root}^*2	193.5	−0.3	3.3	—	78.8	−18.8	111.3	+18.0
				$f(\delta e)$				
$h_s^*0.75$	194.9	+0.4	3.3	−1.0	121.7	+26.3	69.8	−26.0
$h_s^*1.25$	193.2	−0.5	3.3	—	69.0	−28.4	120.8	+28.0

$\tilde{r}_a$	$\tilde{\overline{r}}_b$	$\tilde{r}_d$	$\tilde{\overline{r}}_c$	$\lambda\tilde{E}_\omega$	$\lambda\tilde{E}_d$
8.17	2.2	3185.	149.	5.2	91.2

TABLE 5. (*Continued*)

5 (c) Spruce, rainy days: 169–172

	R_n		G		λE		H	
	$\tilde{R}_n$	$\%R_n$	$\tilde{G}$	$\%G$	$\lambda\tilde{E}$	$\%\lambda E$	$\tilde{H}$	$\%H$
				Standard				
	64.9	—	3.6	—	81.8	—	−20.8	—
				Aerodynamic				
$r_d/2$	65.0	+0.2	3.5	−2.8	100.3	+22.6	−38.9	−87.0
r_a^*2	64.1	−1.1	3.7	+3.7	65.5	−20.0	−5.4	+74.0
$\overline{r_b}/2$, $r_d/2$	65.0	+0.3	3.5	−2.8	87.0	+6.4	−25.5	−22.6
$\overline{r_b^*}2$, r_d^*2	64.5	−0.5	3.7	+3.7	75.1	−8.2	−14.3	+31.3
				Radiation				
$\omega/1.1$	66.9	+3.1	3.6	—	82.5	+0.9	−19.5	+6.4
$\omega^*1.1$	62.0	−4.5	3.6	—	80.7	−1.3	−22.6	−8.8
				Biophysical				
$L_t/2.0$	64.3	−0.9	3.5	−3.7	69.0	−15.6	−8.3	−60.0
$L_t^*1.5$	65.2	+0.4	3.8	+5.6	87.9	+7.5	−26.6	+27.7

$\tilde{r}_a$	$\tilde{\overline{r_b}}$	$\tilde{r}_d$	$\tilde{r}_c$	$\lambda\tilde{E}_\omega$	$\lambda\tilde{E}_d$
12.8	2.6	3306.	99.9	74.0	7.8

to be partitioned proportionately between the sensible and latent heat fluxes.

c. *Turbulent transfer*

Some aspects of the sensitivity of the turbulent transfer description of SiB to uncertainties in the input parameters have already been addressed in Sellers et al. (1986). It will be remembered that G_1, G_2, z_2, z_1, L_d, C_d, p_s and z_{gs} must be specified in order to calculate z_0, d, r_a, $\overline{r_b}$ and r_d. Figures 5, 6 and 7 of Sellers et al. (1986) show the predicted course of variations in z_0 and d with changes in the canopy characteristics, combined together as the bulk canopy drag coefficient, C_D, on the horizontal axis. Figure 13 of this paper shows how the values of r_a, $\overline{r_b}$ and r_d for a specified surface condition under neutral conditions and a constant wind velocity at reference height vary with the same quantity. Table 6 summarizes all of these results in terms of sensitivity of the derived parameter (z_0, d, r_a, $\overline{r_b}$, r_d) to uncertainties/errors in the value of the canopy drag coefficient at the values of 0.01, 0.1 and 0.5; these translate roughly to leaf area indices of 0.05, 1.0 and 10.0, i.e., the range of what is commonly found in nature.

The parameters C_d, p_s, L_d and $(z_2 - z_1)$ contribute linearly to the canopy drag coefficient so it is fairly straightforward to deduce the contribution of uncertainties in each of these quantities to the total error in the output parameters. At this point it is useful to discuss the reasons for, and the likely magnitudes of, the uncertainties in each of these parameters.

The heights of the canopy top and base, z_2 and z_1, and the total leaf area index, L_t, could probably be estimated for a region with a certainty of better than ±50%. The value of C_d is calculated assuming plate-like (or cylinder-like in the case of conifers) behavior of the leaf elements in the airflow with a dependence on the average leaf inclination. Monteith (1973) reproduces data which show the dependence of the leaf drag coefficient on leaf inclination. We have fitted the following simple relationship to this:

$$C_d = (1.328)\frac{2}{\sqrt{\mathrm{Re}}} + 0.45\,\overline{(\sin\theta)}^{1.6} \qquad (25)$$

where

$\overline{\sin\theta}$ sine of mean leaf inclination to airflow

$$= \frac{\int_0^{\pi/2} \frac{1}{2}(1-\chi_L)\cos\xi\,\partial\xi}{\int_0^{\pi/2} \partial\xi}$$

$$= \frac{1}{\pi}(1-\chi_L)$$

ξ leaf azimuth angle
χ_L Ross leaf angle distribution parameter
Re Reynolds number.

Figure 14 shows the predicted variation in the effective element drag coefficient, C_d/p_s with χ_L for a range of leaf area densities. The shelter factor, p_s, is perhaps the least understood of all the input parameters. We have assumed that $p_s = 1$ when the leaf area density is 0, i.e., no shelter effect, and is equal to 4 when the leaf area density is about 6, from the data of Thom (1972).

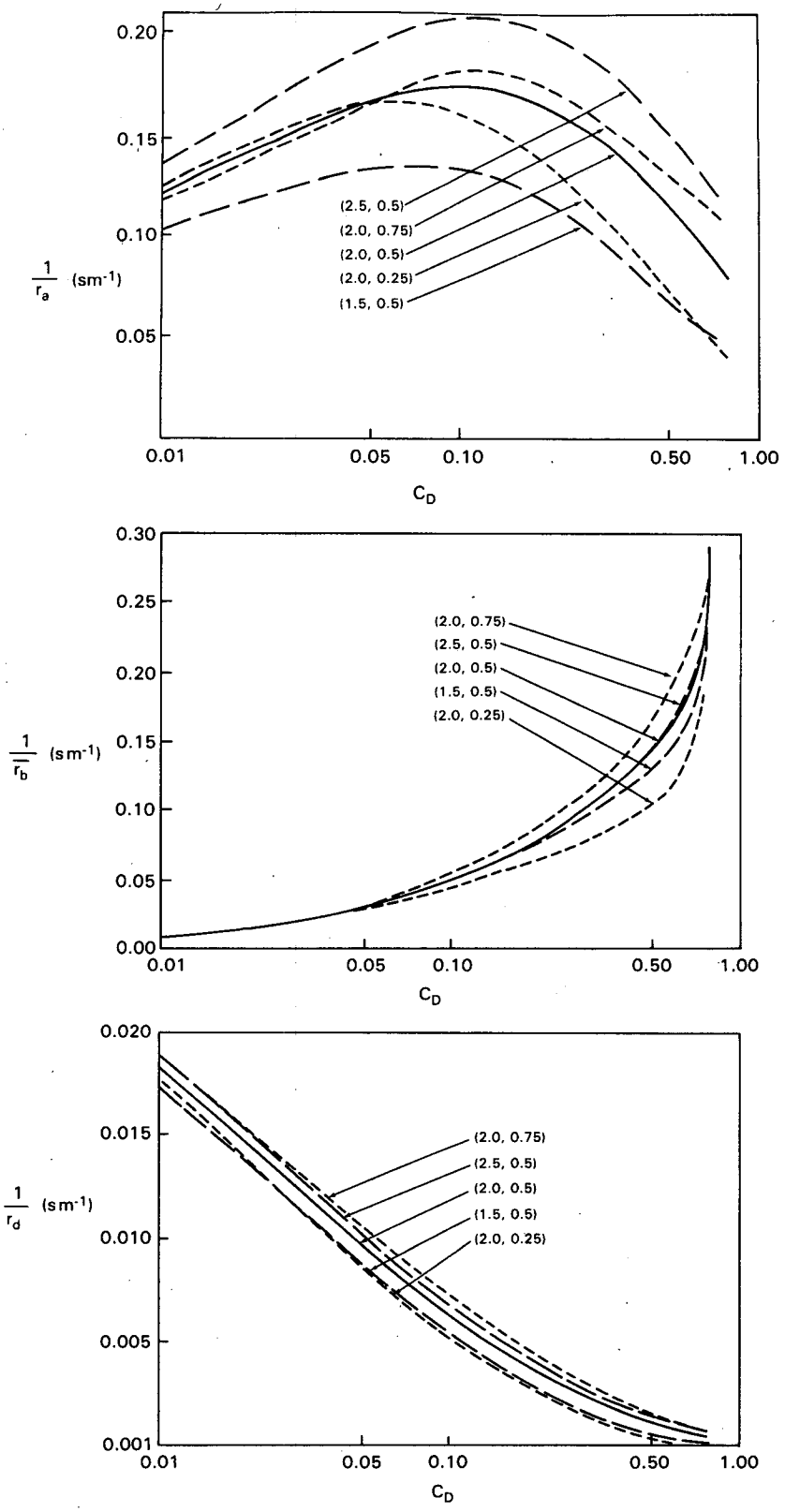

FIG. 13. Variation of the calculated aerodynamic resistances, r_a, $\overline{r_b}$ and r_d, with changes in the values of the adjustment coefficients, G_1 and G_2. In each figure, the values of G_1 and G_2 are specified for individual curves by a pair of numbers in parentheses, with the value of G_1 first and the value of G_2 second. Note that $G_1 = 2.0$ and $G_2 = 0.5$, marked as (2.0, 0.5), represents the default case used in SiB. (a) Variation in the aerodynamic resistance, r_a, with the canopy drag coefficient $C_D(C_D = C_d/p_s L_d(z_2 - z_1))$ for different combinations of G_1 and G_2 values. (b) Variation of $\overline{r_b}$ with C_D for different combinations of G_1 and G_2 values. (c) Variation of r_d with C_D for different combinations of G_1 and G_2 values.

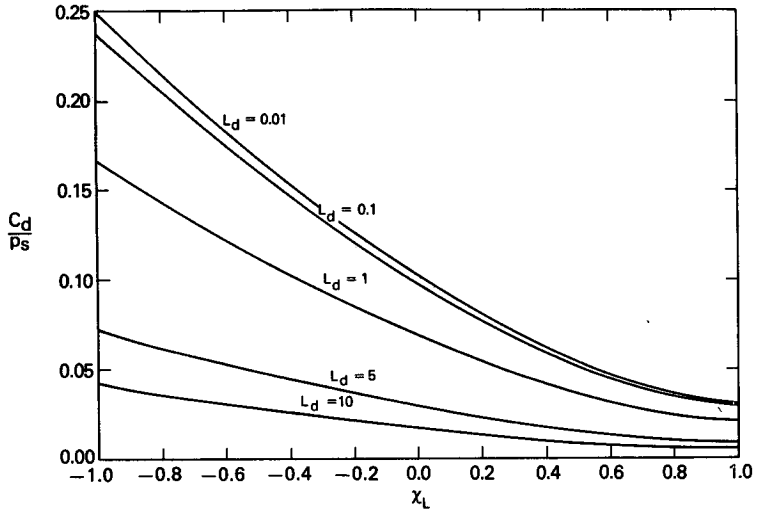

FIG. 14. Variation of effective leaf drag coefficient, C_d/p_s, with Ross leaf angle distribution factor χ_L for a range of leaf area densities, L_d. Values of χ_L of +1, 0 and −1 correspond to horizontal, spherical and vertical leaf orientations, respectively. Formulations governing dependence of C_d, p_s and χ_L are given in the text. (Leaf dimensions: 5 × 5 cm).

Given only these two estimates of p_s, and assuming that it depends linearly on leaf area density, we use

$$p_s = 1 + L_d/2. \tag{26}$$

We can expect from the previous discussion that the errors in the combined term C_d/p_s are somewhere in the region of ±50% again. The total uncertainty in the canopy drag coefficient is therefore likely to be in the region of ±70%. We have taken a range of −50% to +100% about each of the three values of the canopy drag coefficient and have entered the largest resultant error in the output parameters in Table 6a. The uncertainties in the adjustment parameters, G_1 and G_2, are thought to be in the region of ±0.5 and ±0.25 respectively. The combined error resulting from uncertainties in G_1 and G_2 are shown in Table 6b. Lastly, our estimate of the total likely uncertainty in the values of z_0, d, r_a, $\overline{r_b}$ and r_d due to all the errors or uncertainties in the input parameters is shown in Table 6c.

Comparison of Tables 6a, b suggests that the likely sources of error produced by uncertainties in the input parameters are of roughly the same size as those generated by uncertainties in the adjustment parameters G_1 and G_2. In other words, the "fuzziness" in the model's predictive capabilities is comparable to the likely errors in the input data set. Other than that, we find that the fractional error in all the derived quantities increases as the canopy drag coefficient increases, but this is mainly because z_0, $1/r_a$, $1/\overline{r_b}$ and $1/r_d$ all decrease in absolute terms over the same range—the absolute error does not increase so rapidly. Further, zero plane displacement height being insensitive to parameter uncertainties of all kinds, the main sensitivity in $1/r_a$, $1/\overline{r_b}$, and $1/r_d$ follows generically from the value of and uncertainty in z_0.

TABLE 6. Maximum uncertainties, in percent, generated in canopy aerodynamic properties z_0, d, r_a, $\overline{r_b}$ and r_d due to (a) uncertainties in the canopy drag coefficient, C_D, where $C_D = (C_d/p_s)\, L_d(z_2 - z_1)$; (b) uncertainties in the adjustment coefficients, G_1 and G_2; and (c) combined effects of uncertainties in canopy drag coefficient, C_D, and G_1 and G_2, in percent. The calculations were performed for the three values of C_D, 0.01, 0.10 and 0.50, which make up the columns of the table. Here z_0 is the roughness length; d is the zero plane displacement; r_a, r_b and r_d are the aerodynamic, bulk leaf boundary layer and surface to canopy resistances, respectively; z_2 is the height of the canopy. All simulations performed for neutral conditions, z_2 = 5 m and wind speed at 15 m is 10 m s^{-1}.

(a) Canopy drag coefficient, C_d

C_D	0.01	0.10	0.50
z_0/z_2	76	29	58
d/z_2	20	8	13
$1/r_a$	12	5	69
$1/\overline{r_b}$	101	59	51
$1/r_d$	22	42	133

(b) Adjustment coefficients, G_1 and G_2

C_D	0.01	0.10	0.50
z_0/z_2	27	38	54
d/z_2	2	5	9
$1/r_a$	15	24	55
$1/\overline{r_b}$	~5	8	27
$1/r_d$	6	23	82

(c) Canopy drag and adjustment coefficients

C_D	0.01	0.10	0.50
z_0/z_2	81	48	79
d/z_2	20	9	16
$1/r_a$	19	25	88
$1/\overline{r_b}$	101	60	58
$1/r_b$	23	48	156

The total uncertainty in the derived parameters is shown in Table 6c. At first sight, these appear to be unacceptably high, particularly at extreme values of the canopy drag coefficient. Uncertainties in the estimates of z_0 range from 48 to 81%, while those in $1/r_a$, the dominant turbulent transfer term, range from 25 to 88%. The size of these uncertainties should be placed in the context of what is currently used in GCMs to describe surface roughness. Frequently, one value of z_0 is used to describe the roughness of the entire terrestrial surface (Sellers, 1986) while observations and the simple model described previously indicate that it should vary from less than a millimeter to a few meters, depending on the type and amount of vegetation present. (The extreme percentage errors in $1/\overline{r_b}$ and $1/r_d$ occur when both quantities are very, very small.) However, the true test of model sensitivity, rather than single component sensitivity, comes when we place comparable errors in these five derived parameters into the complete SiB model. For these tests, we chose to test errors in r_a, $\overline{r_b}$ and r_d of -50 and $+100$% about the original values calculated by the SiB preprocessor module.

Table 5 shows the resultant errors in the energy balance components: net radiation, $\tilde{R}_n$; ground heat flux, $\tilde{G}$; latent heat flux, $\lambda\tilde{E}$; and sensible heat flux, $\tilde{H}$, produced as a result of errors in the various aerodynamic resistances. The induced changes in the net radiation and ground heat flux terms are negligible. When the canopies are dry (see Tables 5a and 5b), the latent heat and sensible heat flux means show a small sensitivity (7% or less in the case of the latent heat fluxes) to the large input errors in r_a, $\overline{r_b}$ and r_d. When the canopy is wet, however, the errors in the estimates of latent heat flux may grow up to ± 20% (see Table 5c) as here the evaporation is governed solely by the atmospheric forcing and the aerodynamic resistance. It should be pointed out that the results in Table 5c represent an extreme case—in reality, a greatly increased evaporation rate could have a local damping feedback on the evaporative demand by increasing the humidity of the planetary boundary layer. Nonetheless, we may expect that uncertainties in the calculated interception loss rates from tall vegetation may be on the order of ± 20% because of uncertainties in the turbulent transfer description. These results are encouraging as they suggest that the uncertainties and errors in the aerodynamic transfer description and input data may be responsible for relatively small errors in the net radiation and errors of the order of less than 10% in the calculated values of λE and H under dry conditions and somewhere around 20% under wet conditions.

It should be remembered that all of this discussion is based on the results obtained from the Paulson (1970) description of transfer processes in the constant stress layer. Most GCMs use elements of the Paulson (1970) formulation but combine these with descriptions of processes within the planetary boundary layer, plainly beyond the scope of this paper. For the most part we should expect the GCM turbulent transfer descriptions to respond to uncertainties in the surface parameters in approximately the same way as was described here, although there are sure to be some idiosyncratic responses depending on the exact type of formulation used.

d. Biophysical control of evapotranspiration

A number of processes fall under this heading, namely:

leaf stomatal resistance (light dependence), r_s
leaf area index, L_t
plant resistance r_{pl}
root system resistance, r_{root}
soil moisture control of $\overline{r_c}$ through $f(\psi_l)$
vapor pressure deficit control of $\overline{r_c}$ through $f(\delta e)$
interception capacity control of interception loss through S_c.

These are discussed, in turn, in subsections 4d1–4d7.

1) LEAF STOMATAL RESISTANCE, r_s

The expression for the stomatal resistance of an individual leaf is given by (21) in this paper and is discussed in more detail in Sellers (1985). Table 5 shows the effects of increasing or reducing r_s by 25% by multiplying the a and c coefficients in (21) by the relevant fraction. This process merely simulates the effects of changing the light response portion of r_s, independent of the other environmental factors $f(T_c)$, $f(\psi_l)$ and $f(\delta e)$. It is probable that this sensitivity test is overly pessimistic: an error of ± 25% covers the physiological differences between red pine and beech or oak and maize (Turner, 1974). A carefully assembled dataset should be able to quantify these coefficients (for green, healthy leaves) within these limits of uncertainty. It is clear from Table 5 that these relatively large changes in r_s have little effect on the energy balance of the barley crop but have an effect, roughly proportional to themselves, on the calculated latent heat flux from the spruce canopy. The biophysical reasons for this disparity are clear: with short vegetation, like barley, the aerodynamic resistance plays a relatively large role in determining the partitioning of the available energy, $R_n - G$, into λE and H. This is because the effect of changes in $\overline{r_c}$ upon λE, i.e., $(\partial\lambda E/\partial\overline{r_c})$, varies as $-1/(\overline{r_c} + r_a)^2$ and so when r_a and $\overline{r_c}$ are comparable in size ($\tilde{r}_a = 48.9$, $\overline{r_c} = 51.2$ s m^{-1} in the case of barley), the term $\partial\lambda E/\partial\overline{r_c}$ is relatively insensitive to proportional changes in $\overline{r_c}$. When dealing with tall crops, however, $\overline{r_c}$ is the dominant control over the transpiration rate ($\tilde{r}_a = 8.17$, $\tilde{\overline{r_c}} = 149.0$ for the spruce clear day simulations) and so the effects of even small changes in r_s are evident in λE. However, the errors produced in the calculation of the transpiration flux as a result of uncertainties in the r_s coefficients should be limited to or less than the

proportional size of the errors in those coefficients. Hopefully, these uncertainties could be limited to ±15% or less.

2) LEAF AREA INDEX, L_t

The effect of uncertainties in the total leaf area index or in the proportion of live to dead leaves in the canopy on the value of $\bar{r}_c$ was discussed in Sellers (1985). Because of the nonlinear dependence of $\bar{r}_c$ upon leaf area index and the live/dead ratio, the effect of quite large errors in these quantities on the evapotranspiration rate is relatively small, particularly in the case of short crops. In the barley case, the effects of quite large changes in the leaf area index on the energy balance were almost negligible for the reasons previously discussed. In the case of the spruce forest, where the canopy resistance term dominates the partitioning of energy, uncertainties in the leaf area index of ±50% give rise to changes of −24.3 to +19.3% in the estimated transpiration rate. It should be noted that in this particular sensitivity test, the leaf area index affects both the radiation and stomatal resistance submodels but *not* the turbulent transfer description as the standard values of z_0, d, C_1 and C_2 were used. The quite large changes in leaf area index did not affect the net radiation greatly, presumably because even the lowest values of leaf area index used here (about 2.0) were enough to make the surface albedo approach that for an infinitely thick canopy (Sellers, 1985 and Dickinson, 1983). Large errors in the leaf area index may give rise to significant but not proportional errors in the evapotranspiration rate. Because of the nonlinearity of the leaf area index/canopy resistance relationship, the effect of a 50% change in the leaf area index gave rise to a maximum change of less than 25% in the evapotranspiration rate.

3) PLANT RESISTANCE, r_{pl}

There is a large uncertainty in the value of r_{pl}, the resistance imposed by the plants' vascular systems. The simulations summarized in Table 5 indicate that the large errors in the specification of this quantity (−50 to +100%) have little effect on any of the energy balance terms. This is presumably because the root system resistance, r_{root}, with which r_{pl} is combined in summation to calculate the regulation of moisture flow from soil to leaf, is usually the dominant term.

4) ROOT RESISTANCE, r_{root}

This term is calculated by a combination of contributing parameters concerned with root length density, rooting depth, root hydraulic conductivity and soil properties (Sellers et al., 1986). As a result, the uncertainty in r_{root} is large, particularly as this is probably the weakest part of SiB or any other biophysical model because so little is known about root processes. We have applied the usual uncertainties (−50 to +100%) to this quantity and have obtained results that reflect what we already know from the r_s sensitivity analysis; that is, where $\bar{r}_c$ is dominant, the $\bar{r}_c$ related terms are more important. Thus the effect of changes in r_{root} on the estimate of λE in the barley simulations is smaller than that for the spruce simulations. Although the effects of uncertainties in r_{root} are fairly large (of the order of ±15%), they should only have a severe impact when soil moisture is limited.

5) SOIL MOISTURE CONTROL OF $\bar{r}_c$ THROUGH $f(\psi_l)$

Equations (20) to (23) describe how the leaf water potential, ψ_l, may increase the canopy resistance, $\bar{r}_c$. The precise mechanism for this influence is determined by the values of two critical leaf water potentials, ψ_{c_1}, when stomata start to close, and ψ_{c_2}, when the stomata are assumed to be completely closed. When ψ_l falls between these two values as a result of high evapotranspirative demand and/or falling soil moisture potential, $f(\psi_l)$ drops below unity, which is its value when ψ_l has no influence on transpiration. Table 5 shows how changes in ψ_{c_1} and ψ_{c_2} may influence the estimation of the energy balance terms. It is clear that fairly rough estimates of these quantities will suffice, the resulting error $\lambda\tilde{E}$ being comparatively small for large changes in both quantities. It is probable that the specification of ψ_{c_1} and ψ_{c_2} may become more important when the soil moisture is diminished.

6) VAPOR PRESSURE DEFICIT CONTROL OF $\bar{r}_c$ THROUGH $f(\delta e)$

A number of vegetation types, notably the conifers, exhibit the feed-forward response to vapor pressure deficit whereby the stomata progressively close as the ambient air becomes dryer. Table 5b shows the effect of a ±25% uncertainty in the $f(\delta e)$ parameter, h_5, on the calculation of $\lambda\tilde{E}$ and other quantities. It is clear once again that when $\bar{r}_c$ is the dominant term in the $\lambda\tilde{E}$ calculation, errors in its ($\bar{r}_c$) estimation will be more or less equally reflected in $\lambda\tilde{E}$.

7) INTERCEPTION CAPACITY CONTROL OF INTERCEPTION LOSS, S_c

S_c is the estimated maximum amount of intercepted rainwater that can be held by the canopy, currently assumed to be 0.25 mm per unit leaf area index (from Hancock and Crowther, 1979). Table 7 shows the result of making relatively large changes in S_c (±50%) upon the estimation of the total interception loss over a 40-day period for the Norway spruce simulation. The resultant changes in $\lambda\tilde{E}_\omega$ are small, ranging from −13.2% to +7.6%, implying that for this case at least, interception loss is less dependent on the value of S_c than it might at first appear (Sellers et al., 1986). Naturally, under different climatic conditions, we may expect to see a different sensitivity response.

TABLE 7. Sensitivity of time-averaged energy fluxes, resistances and evapotranspiration to changes in the interception capacity, S_c, over a 40-day period at the spruce site. In each case, the second column of figures, labeled with "%," refers to percentage change from the standard run.

	R_n		G		λE		H	
	$\tilde{R}_n$	$\%R_n$	$\tilde{G}$	$\%G$	$\lambda\tilde{E}$	$\%\lambda E$	$\tilde{H}$	$\%H$
Standard	145.9	—	0.3	—	85.4	—	60.1	—
$S_c * 1.5$	145.9	—	0.4	+33	86.2	+0.9	59.4	−1.2
$S_c * 0.5$	145.8	−0.1	0.3	—	84.1	−1.5	61.3	+2.0

	$\tilde{r}_a$		$\tilde{r}_b$		$\tilde{r}_d$		$\tilde{r}_c$		$\lambda\tilde{E}_w$		$\lambda\tilde{E}_d$	
	Mean	%	Mean	%	Mean	%	Mean	%	Mean	%	Mean	%
Standard	11.2	—	3.	—	3180	—	186	—	15.0	—	69.5	—
$S_c * 1.5$	11.2	—	3.	—	3181	—	186	—	17.1	+7.6	69.1	−0.6
$S_c * 0.5$	11.1	−1.0	3.	—	3180	—	186	—	13.8	−13.2	70.3	+1.2

e. *Initialization of prognostic variables*

In SiB, the prognostic variables are the canopy and ground temperatures, T_c and T_{gs}; the canopy and ground vegetation interception stores, M_c and M_g; and the soil moisture storages W_1, W_2 and W_3. In SiB, the soil moisture stores are expressed as wetness fractions, varying between 0.0 (no soil water) to 1.0 (soil pore space filled to capacity). As was discussed in Sellers et al. (1986), the effects of inaccurate initialization of T_c, T_{gs}, M_c and M_g are minor as these variables respond rapidly to changing environmental conditions and have short "memories." The initialization and subsequent values of the soil moisture stores are of far greater importance: the soil can typically store on the order of 100 to 200 mm of water which is available for evapotranspiration (or somewhere around one month's worth of moisture). Clearly, inaccurate specification of the initial soil wetness or poor budgeting of the same could severely affect the calculated partitioning of energy.

Table 8 shows the sensitivity of the energy balance components to initial settings of the soil moisture stores for the barley and spruce clear day sensitivity runs. The two vegetation types show similar trends in their responses to decreasing soil moisture, the differences between them being accounted for by differences in vegetation physiology and soil properties. In both cases we see little change in any of the components until the soil wetness drops below about 0.5, at which point the leaf water potential may drop below ψ_{c_1} for significant lengths of time. Thereafter, we see a rapid decrease in transpiration, with the excess energy being lost as sensible heat and ground heat flux. The vegetation surface warms up as the effects of evaporative cooling fall off and so the net radiation drops due to the increased longwave loss. This result is interesting from a historical viewpoint as it does not compare well with the perfor-

TABLE 8. Sensitivity of the time averaged energy fluxes to changes in soil moisture for (a) the barley site for two sunny days and (b) the spruce site for three sunny days. In each case, the second column of figures, labeled with "%," refers to percentage change from the standard run.

	$\tilde{R}_n$	$\%R_n$	$\tilde{G}$	$\%G$	$\lambda\tilde{E}_d$	$\%\lambda E$	$\tilde{H}$	$\%H$
				(a) Barley				
Standard (0.87)	153.1	—	1.3	—	134.6	—	17.1	—
1.0	153.1	—	1.3	—	134.6	—	17.1	—
0.5	152.7	−0.2	1.4	+3.3	131.7	−2.2	19.6	+14.6
0.4	151.6	−1.0	1.5	+15.4	126.4	−6.0	23.6	+37.6
0.3	150.4	−1.8	1.5	+13.6	114.4	−15.0	34.4	+100.5
0.2	139.9	−8.6	1.7	+29.2	28.7	−78.6	109.4	+539.0
0.1	136.2	−11.1	2.7	+104.1	9.0	−93.3	124.4	+626.0
				(b) Spruce				
Standard (0.71)	194.1	—	3.3	—	96.4	—	94.3	—
1.0	194.1	—	3.3	—	96.4	—	94.3	—
0.5	194.1	—	3.3	—	96.4	—	94.3	—
0.4	193.8	−0.1	3.3	—	86.8	−10.1	103.7	+10.0
0.3	191.0	−1.6	3.4	+3.0	5.7	−94.1	181.9	+92.9
0.2	190.9	−1.6	3.6	+7.0	3.0	−96.9	184.3	+95.5
0.1	190.5	−1.9	4.0	+20.0	0	−100.0	186.5	+98.0

mance of most of the linear "β-functions" commonly used by the general circulation modeling community to date. It is also clear that the correct initialization of soil moisture is fairly crucial for a meaningful prediction of the surface energy balance, particularly when the soil is drying. The problem of obtaining usable global soil moisture climatologies was discussed in Sellers et al. (1986).

5. Summary discussion of model sensitivity

The results of subsections 4d–4e provide us with a means of assessing the suitability of the SiB model for its intended task, the calculation of the surface fluxes for use within general circulation models. It should be noted at this point that these sensitivity studies were executed with fixed upper boundary conditions, the micrometeorological data, and so no feedback effects between the surface and boundary layer could be described. In addition, we have discussed the sensitivity problem only in the context of two vegetation types situated in a temperate (northwest European) environment; obviously, further work needs to be done with different vegetation types in different environments before any final definitive statements can be made about the model performance. Even so, the results we have should provide us with a good indication of what we should expect from the model, and also where we should concentrate our efforts in the data collection for SiB.

The most important findings associated with the sensitivity tests may be summarized as follows:

1) *Total energy balance.* Large errors/uncertainties in all three model subcomponents (radiative transfer, turbulent transfer and biological control of evapotranspiration) have proportionately reduced effects on the total energy available for evapotranspiration and sensible heat, i.e., $Rn - G$. Given that most of the prescribed changes erred on the drastic side, it is reassuring to note that changes in the net radiation were limited to roughly $\pm 7\%$. All of the sensitivity trials (with the exception of those associated directly with radiation interception) indicated that the partitioning of energy into H and λE is the process most sensitive to changes in the model parameters.

2) *Turbulent transfer.* Large changes in all of the components of the turbulent transfer description have little effect on the partitioning of energy *except* when the canopy was wet for a significant part of the time. Normally, the uncertainties in the parameters and the diffusion model itself gave rise to changes in $\lambda\tilde{E}$ of the order of $\pm 5\%$. These rose to $\pm 20\%$ in the case of the spruce forest exposed to almost continuous rainfall. We suspect that the data input to the model would be better than the conservative error estimates used in this study. Also, interception loss rarely amounts to more than 50% of the annual evapotranspiration loss for a region. In view of this, we propose that uncertainties (including variability in the surface condition) in the turbulent transfer description would probably result in an error of roughly $\pm 10\%$ in $\lambda\tilde{E}$.

3) *Biophysical control of evapotranspiration.* The simulations indicate strongly that λE may be very sensitive to the physiological properties of the vegetation, especially in the case of tall vegetation where the aerodynamic resistance, r_a, is small. At worst, errors in the light-dependent coefficients of r_s, in the leaf area index (Sellers, 1985), and in the coefficients controlling the $f(\psi_l)$, $f(\delta e)$ and $f(T)$ responses may generate proportional errors in λE. Additionally, the probable errors in the description of the plant vascular system resistances, r_{pl} and r_{root}, may produce errors of about $\pm 15\%$ in λE. Clearly, these quantities are of crucial importance, all the more so for having been completely overlooked by the GCM community until very recently. A determined data collection effort should be able to reduce the uncertainties in the stomatal response coefficients to something like $\pm 20\%$, but it is unlikely that the vascular parameters, r_{pl} and r_{root}, which are important when the soil is drying, could ever be specified to better than $\pm 50\%$. An inspection of Table 5 shows that these uncertainties are liable to leave us with an almost irreducible uncertainty in λE of roughly $\pm 15\%$.

From the foregoing, we can propose that the errors in the SiB model output due to the uncertainties in the prescribed parameter set are likely to be of the order of $\pm 7\%$ in the calculation of the net radiation and could be as high as $\pm 25\%$ in the calculation of the evapotranspiration flux. It is doubtful whether the latter uncertainty could ever be reduced below $\pm 15\%$ for tall crops. It has been argued that these uncertainties are comparable to what could be achieved with simpler models using far fewer parameters. The analysis presented in Sellers (1986), however, demonstrates that simplistic treatments of the aerodynamic and surface resistance terms can lead to errors in the evapotranspiration calculation on the order of 100% or more. The use of a larger physically based parameter set, even though some of the parameters may have large uncertainties, may thus be vindicated in terms of realism and accuracy.

The previous discussion has been mainly addressed to the modeling of processes at a point or within a small area. When the model is applied to large areas, commensurate with the horizontal resolution of GCMs, more problems arise associated with spatial variability. If we are dealing with a relatively undisturbed biome (such as tropical rain forest, taiga, desert), the challenge is to avoid incorporating biases in the parameter set. We have seen that most of the errors in the parameter set tend to operate more or less linearly in producing resultant errors in the energy balance calculations, so that provided good *mean* values of the parameters are obtained, the SiB system should work reasonably well. However, this assumption cannot be made for the ef-

fects of differential soil moisture contents and root properties, both of which have extremely nonlinear effects on evapotranspiration when the local soil wetness drops below about 0.5. Here the GCM modeler is presented with a clear choice: either retain a grid-scale mean soil wetness and root properties for the calculation of evapotranspiration and acknowledge the inevitable uncertainties in λE as the area dries out, or attempt, using ensemble averaging techniques, to incorporate the effects of soil moisture variability explicitly. In view of the foregoing, it is probable that mean values of most of the SiB parameters will suffice for the grid area calculation with some kind of ensemble averaging process, perhaps utilizing lognormal distributions for the soil wetness and root properties, to account for the nonlinear response of the energy balance to variations in these variables.

6. Summary

The SiB model produced simulations of the energy balances of barley, wheat, maize and Norway spruce sites over periods ranging from 1 to 40 days. Generally, it was found that the model reproduced time series of latent, sensible and ground heat fluxes and surface radiative temperature comparable with the available data. Additionally, the Norway spruce simulation runs produced calculated interception loss rates that compared well with the available observations. It is proposed that the success of the model simulations was due to the relatively realistic description of the biophysical processes associated with energy capture and partition, a result that could only be achieved with a large input parameter set for each vegetation type. The sensitivity of the model to uncertainties and errors in the input parameter set was explored. The likely span of errors to be found in the SiB parameter set would probably give rise to uncertainties in the net radiation absorbed by the surface of ±7%, and uncertainties of up to ±25%, but more generally ±15%, in the estimation of the latent heat flux. Uncertainties in, and the spatial variability of, the soil moisture content were found to be important when the soil moisture drops below roughly 50% of its maximum value for the two test cases studied. The nonlinearity of the effect of differential soil moisture on evapotranspiration may pose some considerable problems when large grid area-averages of the energy flux terms are calculated.

Acknowledgments. Piers Sellers and Jeffrey Dorman work for the Center for Ocean–Land–Atmosphere Interactions (COLA) at the University of Maryland, sponsored by NASA Grant NAG 5-492. The authors wish to extend their thanks to the following for useful discussions and help: A. Dalcher, Y. Mintz, Y. C. Sud, T. J. Schmugge, I. R. Calder, R. Harding, R. J. Gurney, B. J. Choudhury and P. J. Camillo. Drs. Gurney, Choudhury and Camillo are also to be thanked for providing the field measurement data for the agricultural sites for the tests. Dr. Calder and Mr. Harding of the Institute of Hydrology, United Kingdom, are to be thanked for generously providing the Norway spruce data set and many subsequent clarifying discussions. Ms. Joyce Tippett is thanked for typing and editing this paper.

REFERENCES

Arakawa, A., 1972: Design of the UCLA General Circulation Model. Tech. Rep. 7, University of California, Los Angeles, 116.

Calder, I. R., 1976: The measurement of water losses from a forested area using a "natural" lysimeter. *J. Hydrol.*, **30,** 311–325.

——, 1977: A model of transpiration and interception loss from a spruce forest in Plynlimon, Central Wales. *J. Hydrol.*, **33,** 247–265.

——, 1978: Transpiration observations from a spruce forest and comparisons with predictions from an evaporation model. *J. Hydrol.*, **38,** 33–47.

——, and M. D. Newson, 1979: Land-use and upland water resources in Britain—a strategic look. *Water Res. Bul.*, American Water Resources Association, **15**(6), 1628–1639.

Choudhury, B. J., 1983: Simulating the effects of weather variables and soil water potential on a corn canopy temperature. *Agric. Meteor.*, **29,** 169–182.

Clapp, R. B., and G. M. Hornberger, 1978: Empirical equations for some soil hydraulic properties. *Water Resour. Res.*, **14**(4), 601–604.

Deardorff, J. W., 1972: Parameterization of the planetary boundary layer for use in General Circulation Models. *Mon. Wea. Rev.*, **100**(2), 93–106.

Denmead, O. T., 1976: Temperate cereals. *Vegetation and the Atmosphere 2,* J. L. Monteith, Ed., Academic Press, 1–31.

——, and B. D. Millar, 1976: Field studies of the conductance of wheat leaves and transpiration. *Agron. J.*, **68,** 307–311.

Dickinson, R. E., 1983: Land surface processes and climate-surface albedos and energy balance. *Advances in Geophysics,* **25,** 305–353.

——, 1984: Modeling evapotranspiration for three-dimensional global climate models. *Climate Processes and Climate Sensitivity,* J. E. Hanson and T. Takahashi, Eds., Amer. Geophys. Union, *Geophys. Monogr.*, **29,** 58–72.

Frank, A. B., J. F. Power and W. O. Willis, 1973: Effect of temperature and plant water stress on photosynthesis, diffusion resistance and leaf water potential in spring wheat. *Agron. J.*, **65,** 777–780.

Garratt, J. R., 1978: Flux profile relations above tall vegetation. *Quart. J. Roy. Meteor. Soc.*, **104,** 199–212.

Goudriaan, J., 1977: Crop micrometeorology: A simulation study. Wageningen Center for Agricultural Publishing and Documentation, Wageningen, The Netherlands, 249 pp.

Gurney, R. J., and P. J. Camillo, 1984: Modelling daily evapotranspiration using remotely sensed data. *J. Hydrol.*, **69,** 305–324.

Hancock, N. H., and J. M. Crowther, 1979: A technique for the direct measurement of water storage on a forest canopy. *J. Hydrol.*, **41,** 105–122.

——, P. J. Sellers and J. M. Crowther, 1983: Evaporation from a partially wet forest canopy. *Annales Geophysicae,* **1**(2), 139–146.

Jarvis, P. G., 1976: The interpretation of the variations in leaf water potential and stomatal conductance found in canopies in the field. *Phil. Trans. Roy. Soc. London,* **273,** 593–610.

——, G. B. James and J. J. Landsberg, 1976: Coniferous forest. *Vegetation and the Atmosphere 2,* J. L. Monteith, Ed., Academic Press, 171–240.

Kimes, D. S., P. J. Sellers and W. W. Newcomb, 1987: Hemispherical reflectance (albedo) dynamics of vegetation canopies for global

and regional energy budget studies. *J. Climate Appl. Meteor.* (in press).

Korner, G., J. A. Schell and H. Bauer, 1979: Maximum leaf diffusive conductance in vascular plants. *Photosynthesis,* **13**(1), 45–82.

Legg, B. J., and I. F. Long, 1975: Turbulent diffusion within a wheat canopy, II. *Quart. J. Roy. Meteor. Soc.,* **101,** 611–628.

Millar, A. A., M. E. Duysen and E. B. Norum, 1970: Relationships between the leaf water status of barley and soil water. *Can. J. Plant. Sci.,* **50**(4), 363–370.

Monteith, J. L., 1973: *Principles of Environmental Physics.* Edward Arnold Ltd., 242 pp.

——, G. Szeicz and P. E. Waggoner, 1965: The measurement and control of stomatal resistance in the field. *J. Appl. Ecol.,* **2,** 345–355.

Newman, E. I., 1969: Resistance to water flow in soil and plant, I, soil resistance in relation to amounts of root: Theoretical estimates. *J. Appl. Ecol.,* **6,** 1–12.

——, 1973: Permeability to water of the roots of five herbaceous species. *New. Phytol.,* **72,** 547–555.

Paulson, C. A., 1970: Mathematical representation of wind speed and temperature profiles in the unstable atmospheric surface layer. *Quart. J. Roy. Meteor. Soc.,* **89,** 857–861.

Raupach, M. R., and A. S. Thom, 1981: Turbulence in and above plant canopies. *Annual Review of Fluid Mechanics,* **13,** 97–129.

Reicosky, D. C., and J. R. Lambert, 1978: Field measured and simulated corn leaf water potential. *Soil Sci. Soc. Am. J.,* 221–228.

——, R. B. Campbell and C. W. Doty, 1975: Diurnal fluctuation of leaf-water potential of corn as influenced by soil matrix potential and microclimate. *Agron. J.,* **67,** 380–385.

Ross, J., 1975: Radiative transfer in plant communities. *Vegetation and the Atmosphere, 1,* J. L. Monteith, Ed., Academic Press, 13–52.

Sellers, P. J., 1985: Canopy reflectance, photosynthesis and transpiration. *Int. J. Remote Sens.,* **6**(8), 1335–1372.

——, 1987: Modeling effects of vegetation on climate. *The Geophysiology of Amazonia: Vegetation and Climate Interactions,* R. E. Dickinson, Ed., Wiley and Sons.

——, Y. Mintz, Y. C. Sud and A. Dalcher, 1986: The design of a simple biosphere model (SiB) for use within General Circulation Models. *J. Atmos. Sci.,* **43**(6), 505–531.

Shaw, R. H., and A. R. Pereira, 1982: Aerodynamic roughness of a plant canopy: A numerical experiment. *Agric. Meteor.,* **26,** 51–65.

Stewart, J. B., and A. S. Thom, 1973: Energy budgets in a pine forest. *Quart. J. Roy. Meteor. Soc.,* **99,** 154–170.

Thom, A. S., 1972: Momentum, mass and heat exchange of vegetation. *Quart. J. Roy. Meteor. Soc.,* **98,** 124–134.

Turner, N. C., 1974: Stomatal response to light and water under field conditions. *Roy. Soc. N. Z. Bull.,* **12,** 423–432.

Uchijima, Z., 1976: Maize and rice. *Vegetation and the Atmosphere, 2,* J. L. Monteith, Ed., Academic Press, 33–64.

van der Ploeg, R. R., G. Tassone and J. von Hoyningen-Heune, 1980: The Joint Measuring Campaign 1979 in Ruthe (West Germany)—Description of Preliminary Data. European Econ. Comm., Joint Res. Cent., Ispra.

Wilson, J. D., D. P. Ward, G. W. Thurtell and G. E. Kidd, 1982: Statistics of atmospheric turbulence within and above a corn canopy. *Bound.-Layer Meteor.,* **24,** 495–519.